Early Steps in the O2 Scavenger Process in the Aqueous Phase: Hydrazine vs DEHA

Marion Roy, Rahma Dahmani, Valérie Vallet, Michel Masella

Early Steps in the O_2 Scavenger Process in Aqueous Phase : Hydrazine vs DEHA.

Marion Roy,[†] Rahma Dahmani,[‡] Valérie Vallet,[¶] and Michel Masella[*,‡]

[†]*Service d'Etude du Comportement des Radionucléides, Département de Physico-Chimie, CEA Saclay, F-91191 Gif sur Yvette Cedex, France*

[‡]*Laboratoire de Biologie Structurale et Radiobiologie, Service de Bioénergétique, Biologie Structurale et Mécanismes, Institut de Biologie et de Technologies de Saclay, CEA Saclay, F-91191 Gif sur Yvette Cedex, France*

[¶]*Univ. Lille, CNRS, UMR 8523 - PhLAM - Physique des Lasers Atomes et Molécules, F-59000 Lille, France*

E-mail: michel.masella@cea.fr

Abstract

We investigate the first direct proton abstraction reactions from reducing agents (**RAH**) hydrazine and diethyl hydroxylamine (DEHA), towards dioxygen (O_2) in the aqueous phase, spanning ambient to high temperature conditions. Quantum chemistry methods and molecular dynamics simulations are employed in this study. Quantum chemistry methods are used to analyze the quasi-equilibrium between a reactive conformation and a transition state in the [**RAH**,O_2] cluster. On the other hand, molecular dynamics simulations estimate the probability of observing a reactive conformation of the [**RAH**,O_2] cluster in the solution. In this study, we assume that the energy barrier of the quasi-equilibrium is sufficiently high for the **RAH**/O_2 association process to be at equilibrium. Our findings indicate that the first proton abstraction process from a reactive conformation cluster by DEHA is energetically favored compared to hydrazine. Conversely, the association process of hydrazine and O_2 in solution is more favorable than that of DEHA. Consequently, the rate constant for the first proton abstraction process is similar for both hydrazine and DEHA, particularly at high temperatures, with activation energies of approximately $21.5 \pm 1.5\,\mathrm{kcal\,mol^{-1}}$ for both compounds. These results align with recent experiments investigating the complete O_2 scavenger process in liquid water with hydrazine and DEHA. Therefore, our findings support the assumption that first proton abstraction reactions are the rate-determining steps in O_2 scavenger processes in the aqueous phase.

Keywords. Molecular dynamics, quantum chemistry, hydrazine, DEHA, O_2, reactivity, hydration.

1 Introduction

The compound hydrazine (N_2H_4) is an energy-rich molecule commonly utilized as a propellant in spacecraft vehicles and satellites. It also serves as a powerful reducing agent (**RAH**) extensively employed as an O_2 scavenger in water circuits of industrial and power plants.[1] Due to its widespread usage and its toxicity to all living organisms, including humans,[2] there is a pressing need to explore alternatives to hydrazine as a reducing agent. Several alternatives have been investigated, such as carbohydrazide,[3] erythorbic acid,[4] methylethyl-ketoxime,[5] but the compound that has garnered the most interest is diethylhydroxylamine (DEHA).[5–8]

Only scarce and somewhat fragmented experimental data are available regarding the O_2 scavenger process in solution for all the aforementioned **RAH**. Regarding DEHA for instance, two different scavenger mechanisms have been reported. The first mechanism, proposed by Cáceres et al.[6] is based on a rate determining step of first-order kinetics that yields the $HO_2^\bullet$ radical

$$\mathrm{DEHA} + \mathrm{O_2} \rightarrow (\mathrm{CH_3CH_2})_2\mathrm{NO}^\bullet + \mathrm{HO_2}^\bullet \tag{1}$$

The authors reported an apparent activation energy (E_a) for DEHA in chlorobenzene solutions, ranging from 273 to 330 K, to be $16.5 \pm 2.0\,\mathrm{kcal\,mol^{-1}}$.[6] Remarkably, this value aligns closely with the estimated E_a for hydrazine in the aqueous phase at elevated temperatures (from 380 to 573 K) as reported by Buxton and Stuart, which was $16.7 \pm 1.2\,\mathrm{kcal\,mol^{-1}}$.[9] Interestingly, these orders of magnitude for E_a correspond with the energy barrier estimates for the first proton abstraction step of hydrazine in the gas phase, as recently computed by Asgharzade et al. using quantum chemistry methods.[10] Depending on the level of theory employed, the energy barrier ranges from 24 to $30\,\mathrm{kcal\,mol^{-1}}$ when considering O_2 in its most stable triplet state.

Jäppinen et al.[5] recently adopted the aforementioned first-order rate-limiting mechanism to interpret high-temperature kinetic data regarding the O_2 scavenger process of hydrazine, DEHA, and erythorbic acid in a recirculation water loop of a Pressurized Water Reactor (PWR). Their findings revealed that hydrazine exhibited a threefold faster kinetics compared to DEHA at high temperatures (around 573 K).

However, Shaffer and Heicklen[11] proposed a more intricate mechanism for the O_2 scavenger

process of DEHA in the aqueous phase, which relies on the following chain-initiating step:

$$OH^- + O_2 \rightarrow HO_3{}^- \tag{2}$$

$$HO_3{}^- + \text{DEHA} \rightarrow (CH_3CH_2)_2NO^\bullet + H_2O + O_2{}^- \tag{3}$$

$$(CH_3CH_2)_2NO^\bullet + O_2 \rightarrow \text{nitrone} + HO_2{}^\bullet \tag{4}$$

That chain mechanism has recently been reinvestigated, taking into account the DEHA decomposition kinetic in solution,[8] yielding an apparent activation energy $E_a = 14.4\,\text{kcal}\,\text{mol}^{-1}$, which aligns well with the E_a estimation of Ishida et al.[12] for hydrazine in interpreting high temperature data in bulk water (with a consideration of 1 and 0.5 partial orders for hydrazine and O_2), resulting in a value of $10.3\,\text{kcal}\,\text{mol}^{-1}$.

The aim of our study is to combine quantum chemistry methods and MD simulations based on an *ab initio*-based polarizable force field (*i.e.* empirical inter atomic potentials built by considering only quantum chemistry data and no experimental result) to investigate the hypothesis of Cáceres et al. regarding the O_2 scavenger process of hydrazine and DEHA in the aqueous phase for temperatures that range from 300 to 550 K, *i.e.* the scavenger mechanism for both compounds rely on the simple rate limiting step reaction

$$\mathbf{RAH} + O_2 \rightarrow \mathbf{RA}^\bullet + HO_2{}^\bullet \tag{5}$$

Experimental data at high temperatures regarding hydrazine.[5,13,14] show its decomposition rate to be relatively slow, and experiments performed by one of us (MR) show that even DEHA and hydrazine are partially degraded at 423 K during 20 min, a sufficient amount of both compounds is still present in solution (see the Supporting Information). As earlier experimental studies also show the O_2 scavenger kinetics of hydrazine and DEHA to be close and the apparent activation energy E_a for both compounds to be large (≥ 10 kcal mol^{-1}), we assume here the association between the solvated species **RAH** and O_2 to reach equilibrium before proton abstraction to occur.

That yields reaction (5) to obey the following three steps scheme

$$\mathrm{RAH}_s + \mathrm{O}_{2,s} \overset{\text{(a)}}{\rightleftharpoons} [\mathrm{RAH},\mathrm{O}_2]^r_s \overset{\text{(b)}}{\rightleftharpoons} [\mathrm{RAH},\mathrm{O}_2]^\ddagger_s \overset{\text{(c)}}{\longrightarrow} \mathrm{RA}^\bullet_s + \mathrm{HO}_2{}^\bullet{}_s \tag{6}$$

here, the subscript s denotes single species and associated clusters in solution. Step (a) corresponds to the equilibrium (unaltered by any competitive process) between dissociated **RAH** and O_2 species and as associated in a reactive cluster. We define a cluster to be in reactive conformation when the cluster moieties are close enough to each other and in a geometry that favors the proton transfer between them. Step (b) is the quasi equilibrium (according to the Eyring approach) between a cluster $[\mathbf{RAH},\mathrm{O}_2]^r_s$ in a reactive conformation and the transition state $[\mathbf{RAH},\mathrm{O}_2]^\ddagger_s$. Finally step (c) yields the reaction products.

We denote below p_a the probability to observe an associated $[\mathbf{RAH},\mathrm{O}_2]_s$ cluster in solution and we denote p_r the probability for an associated cluster to be in a reactive conformation. Taking the concentration c_0 of **RAH** and O_2 species in solution as equal, the equilibrium constant K_a corresponding to the association of **RAH** and O_2 in solution obeys $K_a = p_a/[c_0(1-p_a)^2]$. From our assumption regarding the efficiency of the reactive step (b), the rate constant $k(\mathrm{T})$ corresponding to a first proton abstraction reaction (5) is

$$k(\mathrm{T}) = \frac{\mathrm{k_B T}}{h} \frac{p_r p_a}{c_0(1-p_a)^2} \exp\left(-\frac{\Delta G^\ddagger_s}{\mathrm{k_B T}}\right), \tag{7}$$

here, $\mathrm{k_B}$ and h are the Boltzmann's and the Planck's constants, respectively.

The quantities p_a and p_r are estimated from MD simulations in the aqueous phase. Regarding p_r the magnitudes of the structural indexes allowing one to identify a potential reactive conformation are defined from optimized quantum chemistry geometries regarding both the reactive $[\mathbf{RAH},\mathrm{O}_2]^r$ and transition state $[\mathbf{RAH},\mathrm{O}_2]^\ddagger$ clusters. We will consider as structural indexes the angle $\xi = \angle(\mathbf{XH},\mathbf{HO})$ and the distance $\mathrm{H}\cdots\mathrm{O}$ (here the XH moiety and atom O belong to **RAH** and O_2, respectively). The free energy barrier $\Delta G^\ddagger$ corresponding to the quasi equilibrium (b) in the aqueous phase will be estimated from high-level *ab initio* CCSD(T) (at the complete basis set limit) and quantum chemistry DFT methods. To account for solvent effects in our DFT computations, we have use the standard Polarizable Continuum Model, PCM, approach.[15]

We will begin by providing a detailed description of the quantum chemistry methods employed,

including the ab initio-based force field utilized to model the microscopic interactions between the solute (hydrazine, DEHA, and O_2) and water molecules. Additionally, we will outline the molecular dynamics (MD) techniques utilized to explore the potential energy surface (PES) of the **RAH**/O_2 system. To validate the accuracy of the force field, we examined the hydration structure and calculated the Gibbs free energy of solvation for each solute, comparing our results with previous experimental and simulation studies. Finally, by considering the quantum energy barriers ($\Delta G^{\ddagger}$) and simulation data for probabilities p_a and p_r, we will discuss the rate constants (k(T)) for the first proton abstraction process of hydrazine and DEHA in solution across a wide range of temperature conditions.

2 Methods

2.1 Quantum chemistry computations

All quantum computations were carried out using the GAUSSIAN-16 package of programs.[16] For the [**RAH**,O_2] clusters, we utilized the DFT UM06-2X functional,[17] along with dispersion corrections D3,[18] and augmented with the aug-cc-pVTZ basis sets.[19,20] To assess the reliability of this level of theory, we extrapolated the cluster binding energies in the gas phase to the Complete Basis Set (CBS) limit using the CCSD(T) level of theory (based on UM06-2X geometries). The CBS extrapolation was performed from CCSD(T)/aug-cc-VXZ calculations (with X = D, T, Q). For the binding energies of hydrated clusters, which were used to assign force field parameters, we employed the PMP2/CBS level of theory with the frozen core approximation. PMP2 (projected Møller-Passet theory) remedies spin contamination problems by applying a spin-projection operator to the unrestricted wave function.[21] It is worth noting that we considered dioxygen O_2 in a triplet state throughout the study. Regarding the **RAH**/O_2 clusters, the spin contamination for standard PMP2 computations was found to be minimal, with a maximum of 3 % (and even less, 0.1 % in the CCSD(T) and UM06-2X calculations).

From UM06-2X/aug-cc-pVTZ computations, we estimate solvent effects on reactive and transition state clusters using the solvent Polarizable Continuum Model[15] approach as implemented in

GAUSSIAN16. The atomic van der Waals radii are 1.83, 1.75, 1.9255 and 1.443 Å for nitrogen, oxygen, carbon and hydrogen atoms, respectively (using the scaling factor 1.1 and the dielectric constant at infinite frequency $\epsilon(\infty)$ is 1.777849). For that purpose we performed a series of computations (for reactive and transition state dimer clusters) in which we set the dielectric constant ϵ_s of liquid water to its experimental value at 1 atm and T = 300, 350, 400, 450, 500 and 550 K (namely, ϵ_s = 78, 63, 49, 40, 35 and 25, respectively).

We discuss in the present study UM06-2X estimates of the differences ΔE and ΔG(T) in absolute energies E and free energies G(T) with respect to reactive clusters. All those ΔE and ΔG(T) estimates are corrected by the differences $\delta E_{\rm CCSD}$ between CCSD(T)/CBS and UM06-2X/aug-cc-pVTZ absolute energy data regarding reactive, transition state and product clusters in the gas phase.

Zero-point energies, ZPE, and thermal corrections to estimate ΔG(T) values are computed according to the harmonic oscillator approximation from UM06-2X frequencies. To account for anharmonicity effects, harmonic frequencies are scaled by the factors proposed by Bakowies and von Lilienfeld [22] for the DFT M06-2X method used in conjunction with the cc-pVTZ basis set (*i.e.* 0.976 and 0.94 for DEHA and hydrazine, respectively). However, as demonstrated by Temelso and Shields [23] for small water clusters, the scaling factor for frequencies lower than 1100 $\rm cm^{-1}$ should be weaker compared to higher frequencies. In light of this, we also considered a scaling factor of 0.85 for frequencies weaker than 1100 $\rm cm^{-1}$.

Our results regarding [**RAH**,O_2] clusters show from 2 (hydrazine) to 5 (DEHA) very low frequencies that span between 10 and 100 $\rm cm^{-1}$. Some of those frequencies correspond to internal rotations. Following the ideas of Zhao and Truhlar [24] we estimate the uncertainty tied to the use of the harmonic oscillator approximation by computing two sets of thermal corrections : the first set is computed from the scaled harmonic frequencies regardless of their magnitude (those corrections are denoted $G_{\rm thermal}$), whereas the second set is computed by raising all the scaled frequencies weaker than 100 $\rm cm^{-1}$ to 100 $\rm cm^{-1}$ (those corrections are denoted $\tilde{G}_{\rm thermal}$). We assume the uncertainty of our free energy ΔG(T) values to correspond to the absolute difference between $\Delta G_{\rm thermal}$ and $\Delta \tilde{G}_{\rm thermal}$ data. Note those thermal corrections are dominated by their vibrational components : the magnitude of their rotational components is one order of magnitude weaker compared to the

vibrational one.

2.2 The polarizable force field

The total potential energy U is the sum of six terms:

$$U^{ww} = U^{rep} + U^{qq'} + U^{pol} + U^{hb} + U^{disp} + U^{rel}. \tag{8}$$

The repulsive U^{rep}, Coulombic $U^{qq'}$, and dispersion U^{disp} terms are defined as

$$U^{rep} = \sum_{i=1}^{N} \sum_{j=1}^{N^*} a_{ij} \exp\left(-b_{ij} r_{ij}\right), \tag{9}$$

$$U^{qq'} = \sum_{i=1}^{N} \sum_{j=1}^{N^*} \frac{q_i q_j}{4\pi\epsilon_0 r_{ij}}, \tag{10}$$

$$U^{disp} = -\sum_{i=1}^{N} \sum_{j=1}^{N^*} \left(\frac{r^*_{ij}}{r_{ij}}\right)^6. \tag{11}$$

N is the total number of atoms, r_{ij} is the distance between the atomic centers i and j, q_i are atomic static charges, and a_{ij}, b_{ij} and r^*_{ij} are adjustable parameters. The repulsive term U^{rep} is truncated for distances larger than 5.0 Å. Dispersion effects are only accounted for to model interactions between non-hydrogen atoms. The sums corresponding to the superscript * include only pairs of atoms separated by more than two chemical bonds.

The energy term U^{rel} corresponds to intramolecular degrees of freedom, like the O–O bond or the dihedral angles H–NN–H of hydrazine. It is the sum of the standard stretching, bending and dihedral torsional energy terms, whose analytical forms are those of the CHARMM force field.[25]

The polarization energy term U^{pol} is defined as

$$U^{pol} = \frac{1}{2} \sum_{i=1}^{N_\mu} \frac{p_i^2}{\alpha_i} - \sum_{i=1}^{N_\mu} \mathbf{p}_i \cdot \mathbf{E}_i^q - \frac{1}{2} \sum_{i=1}^{N_\mu} \sum_{j=1}^{N_\mu^*} \mathbf{p}_i \mathbf{T}_{ij} \mathbf{p}_j. \tag{12}$$

Only the N_μ non-hydrogen atoms are taken as polarizable centers and their isotropic polarizability

is α_i. The induced dipole moments $\mathbf{p}_i$ obey

$$\mathbf{p}_i = \alpha_i \cdot \left(\mathbf{E}_i^q + \sum_{j=1}^{N_\mu^*} \mathbf{T}_{ij} \cdot \mathbf{p}_j \right). \tag{13}$$

$\mathbf{T}_{ij}$ is the dipolar interaction tensor and $\mathbf{E}_i^q$ is the electric field generated on the polarizable atom i by the surrounding static charges q_j. $\mathbf{T}_{ij}$ and $\mathbf{E}_i^q$ include a Thole-like[26] short-range damping component.

The many-body anisotropic short-range energy term U^{hb} was originally introduced to accurately model hydrogen bond, HB, networks among water molecules, see its most recent version TCPE/2013.[27] For our present study, we extend that approach to model hydrazine/DEHA - water HBs. The analytical form of U^{hb} is

$$U^{hb} = \sum f(r) g(\theta, \phi). \tag{14}$$

The sum runs over all the possible **RAH**/water HBs. The HB lengths r_{hb} and the angles θ and ϕ are defined in Figure 1.

The functions f and g are Gaussian or a product of Gaussian functions :

$$f(r) = D_e \exp\left[-\frac{(r_{hb} - r_{e,hb})^2}{\gamma_r} \right] \quad \text{and} \quad g(\theta, \phi) = \exp\left[-\frac{(\theta - \theta_e)^2}{\gamma_\theta} \right] \times \exp\left[-\frac{(\phi - \phi_e)^2}{\gamma_\phi} \right]. \tag{15}$$

$r_{e,hb}$, θ_e, ϕ_e, γ_r, γ_θ and γ_ϕ are adjustable parameters. To account for environmental effects on the magnitude of a particular HB, D_e is taken as a linear function of the local density ρ_{xh} of X-H bonds (X = N or O) in the vicinity of the moiety that accepts hydrogens in HBs (see Figure 1). $D_e = d_e(1 - \xi\rho_{xh})$, with d_e and ξ two adjustable parameters depending on the nature of the hydrogen acceptor moiety. The local density ρ_{xh} is estimated according to

$$\rho_{xh} = \sum \exp\left[-\frac{(r_{hb} - r_{e,hb})^2}{\gamma'_{rt}} \right]. \tag{16}$$

The sum runs on X−H bonds not involved in the HB, see Figure 1.

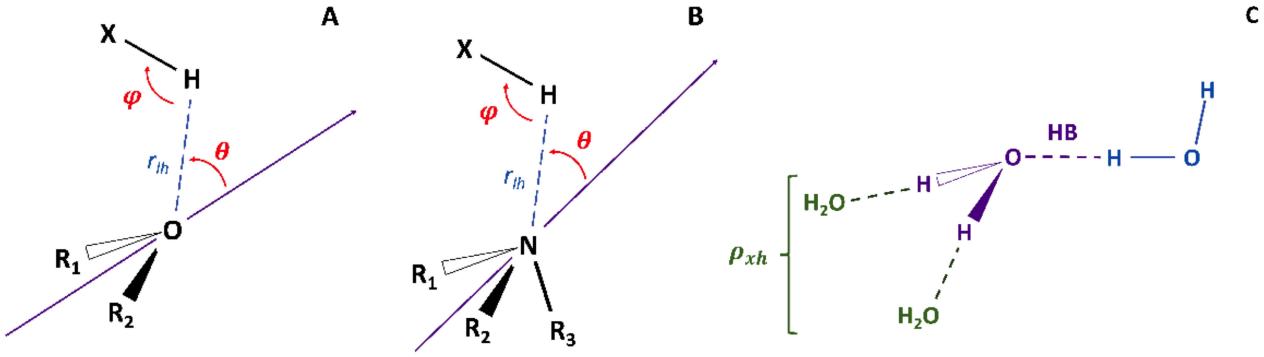

Figure 1: Definition of the HB geometrical parameters of the energy term U^{lh}. **A** and **B**: definition for sp^3 oxygen and nitrogen proton acceptor molecules, respectively. The violet vectors connect the center of mass of the R_i groups to the O/N proton acceptor atoms. **C** : definition of the water molecules that are accounted for to compute the local density ρ_{xh} for the violet water molecule in order to modulate the strength of the HB between the violet and blue water molecules.

2.3 Force-field parameters

The geometrical parameters (bond distances and angles) for intramolecular stretching and bending energy terms for hydrazine and the ethanol amine NOH moiety are shown in Figure 2 and the corresponding harmonic stretching and bending constants are set to best reproduce the harmonic vibrational spectra of isolated hydrazine and DEHA monomer from quantum MP2/aug-cc-pVTZ computations. The remaining set of geometrical parameters (to model DEHA ethyl groups, for instance) correspond to those of the CHARMM v2.7 force field.[25]

The dihedral torsional energy term corresponds to the standard three cosine function sum

$$U^{tor} = V_1 \cos(\omega) + V_2 \cos(2\omega) + V_3 \cos(3\omega)\,. \tag{17}$$

V_{1-3} are adjustable parameters and ω is a standard 1-4 intramolecular dihedral angle. For our purpose all the U^{tor} parameters have been assigned to best reproduce torsional energy profiles from quantum MP2/aug-cc-pVTZ computations (see also Figures S1 and S2 of the Supporting

Information). In the particular case of hydrazine and as already proposed by earlier authors,[28] we define two kinds of hydrogens H and H_2. The hydrazine torsional energy term is a function of only the dihedral angle H_2-NN-H_2 (see Figure 2 for definition). The best values of the hydrazine torsional parameters V_1 to V_3 are 1.0, 5.4 and 1.2 kcal mol^{-1}, respectively.

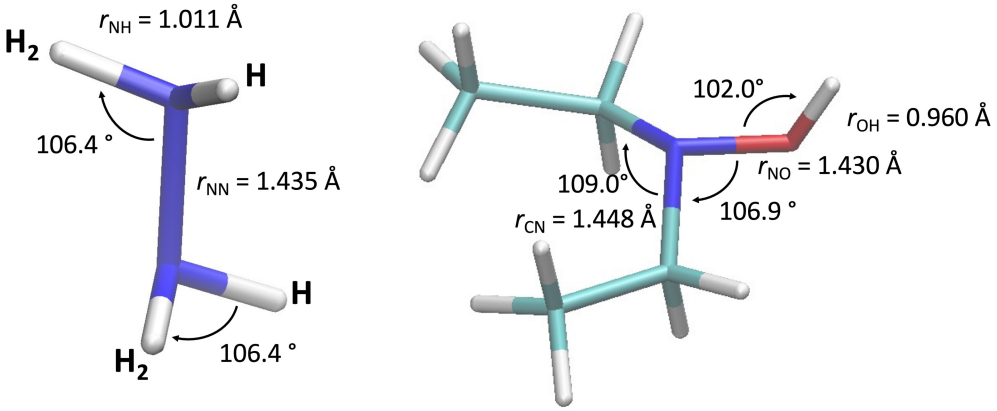

Figure 2: Geometrical data for hydrazine and DEHA. For hydrazine, the definition of its hydrogens H_2 used to compute its dihedral energy component are shown. The Coulombic charges of hydrazine are -0.56 (N) and 0.28 (H) For DEHA, the Coulombic charges of its ethanol amine moiety are -0.14 (N), -0.40 (O), +0.30 (H), and -0.02 for the carbons connecting the ethyl groups to the ethanol amine one and -0.21 for the remaining carbons. The charge for all DEHA aliphatic hydrogens is +0.07. All charges in e. The isotropic polarizabilities for hydrazine nitrogens are set to 1.73 Å^3, whereas they are 2.1 (C), 1.5 (N) and 1.3 (O) Å^3 for DEHA.

Water is modeled according to the original TCPE/2013 model.[27] We assign the parameters corresponding to hydrazine/DEHA - water intermolecular interactions in two steps. First we adjusted repulsive, polarization damping and hydrogen bonding energy parameters to best reproduce quantum MP2/CBS data regarding small ammonia and methanol homo clusters as well as and ammonia/water and methanol/water hetero clusters. Then we refine this starting set of parameters to reproduce our quantum data regarding small hydrazine/DEHA - water clusters (comprising up to four water molecules, see Figures S3 to S4 and Tables S1 to S2 of the Supporting Information).

We set the O_2 inter oxygen distance d_{O_2} to 1.22 Å (its equilibrium distance from quantum computations) and the corresponding stretching harmonic constant to 300 kcal mol^{-1} Å^{-2} (note that we systematically constrain the d_{O_2} distance along our simulations). We do not account for

dioxygen O_2 as computing Coulombic interactions (the O_2 Coulombic charges are set to zero). However, O_2 is a polarizable molecule (its oxygen polarizability is set to $0.675\,\text{Å}^3$ to reproduce its molecular polarizability in the gas phase,[29] $1.35\,\text{Å}^3$). The polarization damping, repulsive and dispersion parameters to model water (or **RAH**) - O_2 interactions are assigned to best reproduce our quantum PMP2 geometrical and binding energy data regarding water/hydrazine-O_2 hetero dimers, as well as the dimer dimethyl hydroxyl amine DMHA/O_2 for efficiency reasons. Quantum energy and geometry data are compared to force field ones regarding O_2-based hetero dimers in Figure 3.

All the force field parameters assigned for the present study are summarized in the Supporting Information.

2.4 MD simulation details

Bulk MD simulations are performed using boundary periodic conditions in the NPT ensemble. The temperature and pressure are monitored using the Nosé-Hoover barostat[30] (the barostat coupling constant is set to 2.5 ps). The simulated systems correspond to cubic boxes that comprise about 1000 water molecules and a single **RAH**/O_2 species or a single [**RAH**,O_2] pair (that corresponds to a 0.05 M scale aqueous solution). All the X−H bond lengths (as well as the O_2 bond length) and all the H−X−H bending angle values are constrained using the RATTLE procedure (the convergence criterium is set to 10^{-5} Å). Electrostatic (Coulombic and polarization) energies and forces are computed according to a lattice-based Smooth Particle Mesh Ewald, SPME, summation approach[31] (the direct term cut off distance, the grid dimension and the expansion order are set to 12, 1 and 8 Å, respectively). The induced dipole moments are solved iteratively until the mean difference in their values between two successive iterations is smaller than 10^{-6} Debye and the maximum difference for a single dipole is smaller than 25×10^{-6} Debye.

The equations of motion are solved using a Multiple Time Steps, MTS, algorithm devoted to polarizable force field based on induced dipole moments.[32] Three time steps are used : 0.25 fs (stretching and bending intramolecular forces), 1 fs (torsional and short-range Coulombic and polarization forces) and 5 fs (long-range Coulombic and polarization forces). The cutoff distance to compute short-range forces is set to 8 Å.

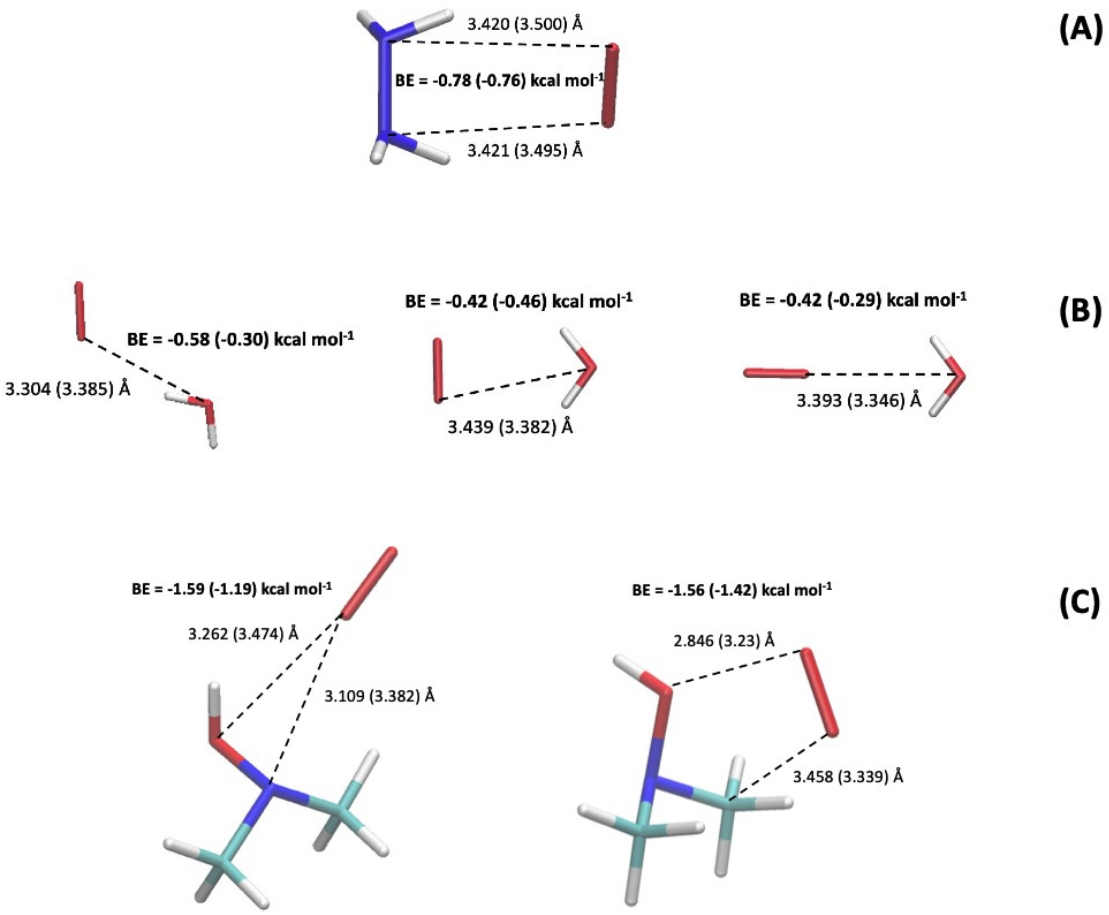

Figure 3: Quantum and force field data regarding binding energies (BE) and geometries of hydrazine/O_2 (A), water/O_2 (B) and DMHA/O_2 (C) hetero dimers.

All molecular modeling computations and simulations were performed with our own code POLARIS(MD).[33]

2.5 Hydration free energy computations

Gibbs hydration free energies ΔG_{solv} of the solutes O_2, DEHA and hydrazine are computed in two steps using a 20 windows Thermodynamical Integration, TI, scheme.[34] Each TI MD simulation is performed at the 10 ns (O_2 and hydrazine) and 20 ns (DEHA) scale. The potential energy derivatives are computed each 250 fs. The first step consists in linearly downscaling to zero the solute charges and polarizabilities. During the second step, all the solute atoms (that correspond now to uncharged and non-polarizable centers) are linearly transformed into ghost centers fully decoupled from the solvent. During that step and to prevent numerical instabilities,[35] inter atomic distances r_{ij} are incremented by the quantity $1-\lambda$ as computing the repulsive, dispersion and hydrogen bond energy terms. λ is the scaling parameter monitoring the progressive downscaling of solute/solvent interactions in the TI scheme.

Our values ΔG_{solv} account for the ideal gas compression correction δG_{rf} to match the usual experimental reference state ($1\,\text{mol}\,\text{L}^{-1}$) as measuring Gibbs hydration free energies. At 300 K δG_{rf} amounts to $\text{RT}\ln\left(\text{V}^0\right) = +1.90\,\text{kcal}\,\text{mol}^{-1}$ (V^0 is the molar volume of an ideal gas).

2.6 PMF computations

The Potentials of Mean Force, PMFs, of a **RAH**/O_2 pair in the aqueous solution are computed according to a MD-based umbrella sampling protocol. The degree of freedom R restrained during these simulations, using the harmonic potential $k_c\left(R-R_c\right)^2$, is the distance between the centers of mass of hydrazine and O_2, and the distance between the DEHA oxygen and the center of mass of O_2. k_c is set to 5 kcal mol^{-1} Å^{-2}. The target distances R_c are regularly spaced by 0.5 Å and they span from 2.0 up to 12.0 Å. The duration of each MD simulation is set to 10 ns. The distances R are sampled each 50 fs. The PMFs are computed by post-processing the set of sampled distances using the Umbrella Integration method.[36] They account for the entropic correction $2\text{RT}\ln\left(R\right)$.

2.7 Clustering

To identify the main **RAH**/O_2 conformations along a MD trajectory, we define a 5 (hydrazine) and 7 (DEHA) dimension vector **V** corresponding to

1. the four hydrazine hydrogen - O_2 distances and the angle $\Psi_{\text{hydrazine}}$ between the hydrazine NN and O_2 axes ;

2. the three sets of the two distances between DEHA oxygen, nitrogen and alcoholic hydrogen and O_2 oxygens, and the angle value Ψ_{DEHA} between the DEHA OH bond and the O_2 axis.

For distances corresponding to the same definition (as the two DEHA oxygen/O_2 distances) they are sorted out from the smallest to the largest values and then stored in **V**. We systematically consider the absolute value of the scalar product to compute the angles Ψ. The set of vectors **V** from sampled MD snapshots are post-processed using the clustering algorithm detailed in Ref. 37 (the maximum number of clusters is set to 20).

3 Results and discussion

3.1 Hydrazine, DEHA and O_2 hydration properties from MD simulations

Here we discuss data from NPT MD simulations regarding the hydration of each single species hydrazine, DEHA or O_2, in the aqueous phase at a temperature ranging from 300 to 550 K. Note that the water model TCPE/2013 is able to reproduce bulk liquid water properties within a large range of temperature conditions at ambient pressure, in particular up to the water critical point (that TCPE/2013 predicts to lie at 653 ± 14 K).[27] All the error bar magnitude mentioned below are computed from the root mean square deviation of a quantity averaged over 1 ns MD segments (starting once the first 1 ns segment of a simulation is achieved).

3.1.1 Hydration Structures

In Figure 4, we present a series of normalized radial distribution functions $g(r)$ and their corresponding integrals $n(r)$ for different solute/water distances. These plots provide insights into the spatial arrangement of water molecules around the solute. From the integrals $n(r)$, we calculate the mean coordination number $\bar{N}_c$, which represents the average number of water molecules within a distance smaller than the position of the first minimum (denoted $\mathbf{M_1}$) of the $g(r)$ functions. The uncertainty associated with the $\bar{N}_c$ values is determined by the difference in $n(r)$ values between the position of $\mathbf{M_1}$ and the closest position where $g(r)$ exceeds its value at $\mathbf{M_1}$ by 5 %.

All the functions $g(r)$ present at short distances a first peak whose height decreases as the temperature increases (and which can even disappear at the highest temperature 550 K). That yields a systematic reduction of $\bar{N}_c$ values as the temperature rises.

Regarding O_2, its oxygens - water oxygens functions $g(r)$ are characterized by a first broad peak centered at 3.4 ± 0.1 Å and the location of their first minimum $\mathbf{M_1}$ is consistently found at 5.2 ± 0.1 Å, regardless of the temperature. The mean coordination number $\bar{N}_c$ of O_2 decreases as T increases from 16.2 ± 0.9 (300 K) down to 12.2 ± 0.8 molecules (550 K). Interestingly, the magnitude of $\bar{N}_c$ for O_2 at ambient conditions is comparable to that of methane (for which the reported values of $\bar{N}_c$ range from 18 to 22 ± 1 molecules[38,39]). Visual analysis of our MD trajectories reveals that O_2 is predominantly surrounded by water molecules in clathrate-like cages, similar to methane, and a small fraction of water hydrogen atoms point towards the oxygen atoms of O_2 throughout the temperature range.

The nitrogens - water oxygens functions $g(r)$ for hydrazine are rather complex at short range. They display two small peaks spanning from approximately 2.8 to 3.6 ± 0.1 Å, followed by a relatively flat minimum at around 5.0 ± 0.5 Å, which we refer to as $\mathbf{M_1}$. The mean coordination numbers $\bar{N}_c$ for the nitrogens of hydrazine are similar in magnitude to those of O_2, regardless of temperature. However, due to the flatness of the $g(r)$ functions near $\mathbf{M_1}$, the uncertainties in $\bar{N}_c$ are large, approximately ±3 molecules.

The radial distribution functions $g(r)$ between the hydrazine hydrogens and water oxygens exhibit two distinct peaks. The first peak is centered at approximately 2.0 ± 0.1 Å, indicating the presence of hydrogen bonds formed between hydrazine hydrogens and water molecules

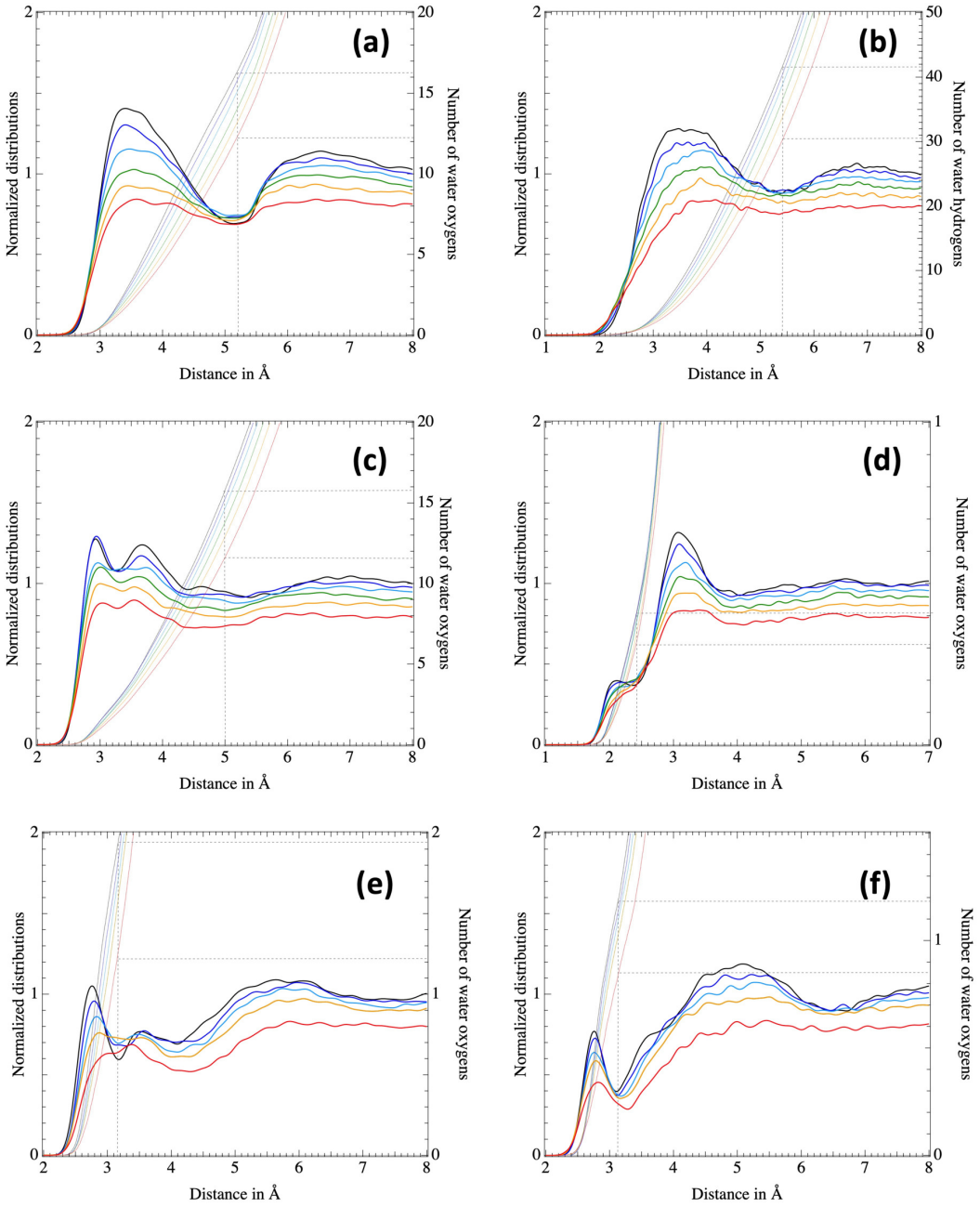

Figure 4: Radial distribution functions (bold lines, left axis)) and their integrals (dashed lines, right axis) corresponding to (a) O_2 oxygens - water oxygens, (b) O_2 oxygens - water hydrogens, (c) hydrazine nitrogen - water oxygens and (d) hydrazine hydrogens - water oxygens, (e) DEHA oxygen - water oxygens and (f) DEHA nitrogen - water oxygens. In black, dark blue, light blue, green, orange and red : data corresponding to 300, 350, 400, 450, 500 and 550 K, respectively. The vertical grey dashed lines are located at the distribution function minima discussed in the main text. For readability purpose, the radial distribution functions are all scaled by the water density at ambient conditions (0.0331 molecule$Å^{-3}$ for the water model TCPE/2013[27]) and the original raw data are smoothed by a 20 windows binomial smoothing scheme.

($H_{hydrazine} \cdots O_{water}$). The second peak, located at around 3.2 ± 0.2 Å, has a height that is two to three times higher than the first peak. The average number of these hydrogen bonds per hydrazine hydrogen decreases from 0.4 at 300 K to 0.30 ± 0.05 at 550 K. On average, hydrazine hydrogens are involved in less than half of a hydrogen bond with water molecules.

Regarding DEHA, the first peaks at short range of its oxygen/nitrogen-water oxygens functions $g(r)$ are noticeably smaller than for both the other species (and that first peak for DEHA oxygen even vanishes at 550 K, see Figure 4). The DEHA coordination numbers $\bar{N}_c$ are thus weak : they decrease from about 1.9 to 1.2 molecules (DEHA oxygen) and from about 1.2 to 0.8 molecules (DEHA nitrogen) as the temperature increases (the $\bar{N}_c$ uncertainties are weak, about 0.1 water molecules). The presence of ethyl groups near the reactive hydroxyl amine moiety of DEHA limits the interaction with water molecules at short distances. This accounts for the smaller coordination numbers observed. On the other hand, the reactive hydrogen - water oxygens $g(r)$ functions show that water molecules establish slightly stronger hydrogen bonds with the DEHA reactive moiety compared to hydrazine. The $\bar{N}_c$ values, representing the average number of DEHA/water hydrogen bonds, decrease from approximately 0.85 to 0.5 ± 0.1 as the temperature increases. These values are roughly twice as large as those observed for hydrazine.

Our $\bar{N}_c$ values for hydrazine, considering their large uncertainties, are in agreement with the earlier data reported by Kallikragas et al.[40] using a standard pairwise force field. For example, Kallikragas et al. showed that $\bar{N}_c$ for hydrazine nitrogens decreases from 11.4 at 298 K to 7.0 at 573 K. However, it is not possible to make a direct comparison between their data and ours, as the uncertainty estimates for their $\bar{N}_c$ values were not provided. It is worth noting that our radial distribution functions $g(r)$ are similar to those reported by Kallikragas et al., although their hydrazine nitrogen functions show a single broad peak at short range rather than two distinct peaks. This difference could be attributed to the use of the directional energy term U^{lh} to model hydrazine/water hydrogen bonds in our simulations.

Our functions $g(r)$ for O_2 are consistent with those reported from simulations using pairwise force fields such as the study by Thapa and Adhikari[41]. However, there have been only a few MD simulation or quantum chemistry studies specifically investigating the hydration of the DEHA hydroxylamine moiety. Most studies have focused on the hydroxylamine molecule (NH_2OH), such

as the works by Vizoso et al.[42] and Ferreira de Lima et al.[43]. It is also worth mentioning a recent study that examined the interaction of DEHA with a single water molecule in the gas phase.[44] In a pioneering work, Vizoso et al.[42] developed pairwise force fields based on *ab initio* quantum chemistry data to investigate the hydration structure of NH_2OH in liquid water at ambient conditions. However it is difficult to directly compare our results for DEHA with those of Vizoso et al. for NH_2OH since the functions $g(r)$ computed from their different force fields already significantly differ from each other.

3.1.2 Hydration energies

The Gibbs hydration energies ΔG_{solv} of O_2, hydrazine and DEHA from our TI simulations at ambient conditions amount to -6.9, +2.9 and -11.5 $\pm$ 0.2 kcal mol^{-1}, respectively. All those ΔG_{solv} values are already converged from 3 ns simulations (see Figure S8 of the Supporting Information).

For hydrazine, our estimate agrees with the most recent experimental data, -6.3 kcal mol^{-1}.[45] Regarding O_2, our ΔG_{solv} estimate is included within the range of available data, for instance: $+1.76\,\mathrm{kcal\,mol^{-1}}$ (from pairwise force field-based simulations,[46] that value doesn't account *a priori* for the reference state correction $\delta G_{\mathrm{rf}} = +1.9\,\mathrm{kcal\,mol^{-1}}$), $+2.0\,\mathrm{kcal\,mol^{-1}}$ (experimental, cited in Ref. 47) and $+6\,\mathrm{kcal\,mol^{-1}}$ (as computed from the O_2 experimental solubility in water[48]).

As far as we know, no experimental ΔG_{solv} estimate for DEHA is available. However assuming hydration enthalpies to be about 30 to 40 % larger in magnitude than free energies for neutral compounds (for instance, the hydration enthalpy and free energy of water are about -10 and $-6\,\mathrm{kcal\,mol^{-1}}$, respectively), our DEHA ΔG_{solv} estimate is in line with the magnitude of the DEHA hydration enthalpy value that may be computed from the DEHA solubility (0.28 in log scale according to the empirical Crippen's method[49]) and from the sublimation and vaporization enthalpies of the pure DEHA compound (12.66 and $3.16\,\mathrm{kcal\,mol^{-1}}$ from experiment[50] and the empirical Joback method,[51,52] respectively) .

3.2 First proton abstraction reactions from quantum chemistry methods

We investigated using quantum chemistry methods the following first proton abstraction reactions of **RAH** towards O_2 in the gas phase and in the aqueous phase

$$[N_2H_4, O_2]^r \rightarrow [[N_2H_3 \cdots H \cdots O_2]^\ddagger \rightarrow [N_2H_3{}^\bullet, HO_2{}^\bullet]^p \tag{18}$$

$$[(CH_3CH_2)_2NOH, O_2]^r \rightarrow [(CH_3CH_2)_2NO \cdots H \cdots O_2]^\ddagger \rightarrow [(CH_3CH_2)_2NO^\bullet, HO_2{}^\bullet]^p. \tag{19}$$

We first investigated the effect of the spin multiplicity on the initial steps of reactions (18) and (19). It was found that in the gas phase, both the reactive and transition state clusters in a singlet state have higher energy compared to their triplet state counterparts by a minimum of $30\,\mathrm{kcal\,mol^{-1}}$. Therefore, for the purpose of the study, singlet state clusters were disregarded, and the focus was solely on triplet state clusters. The data discussed below correspond to these triplet state clusters.

The optimized geometries of clusters corresponding to the reactive [**RAH**,O_2]^r, transition state ([**RAH**,O_2]‡ and product [**RA**$^\bullet$, $HO_2^\bullet$]^p clusters are shown in Figure 5 (cluster Cartesian coordinates are provided in the Supporting Information). Absolute energies ΔE and free energies ΔG(T) (which include ZPE and thermal corrections) of transition state and product clusters *wrt* the reactive ones are summarized in Table 1. In the gas phase :

1. In hydrazine and DEHA transition state clusters, the X $\cdots$ H $\cdots$ O bridge is almost linear (the angle ξ between the vectors **XH** and **HO** is smaller than 20°) and the distances X $\cdots$ H and H $\cdots$ O are close (about 1.22 ± 0.03 Å) ;

2. In reactive clusters, the angle ξ is more distorted (it is about 65 and 35° for hydrazine and DEHA, respectively), and the distance XH $\cdots$ O is twice as large than in transition state clusters (about 2.3 and 2.6 Å for hydrazine and DEHA) ;

3. The geometry of hydrazine evolves towards an almost planar conformation in the product cluster. We note the same trends for DEHA hydroxyl amine moiety but in a lesser extend: its improper dihedral angle ∠CCNO evolves from 65° (reactive cluster) to 29° (product cluster).

From analysis of the spin density, the two species composing the product clusters are radicals (with the spin density maximum equally located on the NO moiety for DEHA) ;

4. The magnitude of the absolute energies $\Delta E^{\ddagger}$ for both **RAH** in the gas phase is large ($\geq$ $+22\,\mathrm{kcal\,mol^{-1}}$). However, it is noticeably weaker for DEHA compared to hydrazine, by $+5.2\,\mathrm{kcal\,mol^{-1}}$.

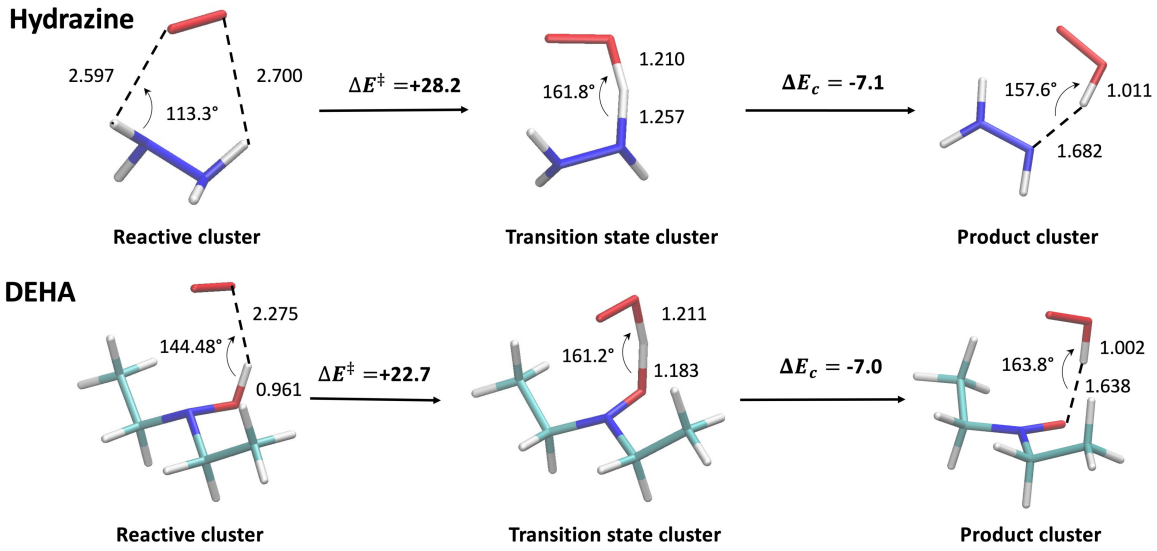

Figure 5: Reactive, transition state and product cluster geometries in the gas phase from quantum chemistry computations. The distances and the difference in gas phase energy (in bold characters) are expressed in Å and $\mathrm{kcal\,mol^{-1}}$, respectively. ΔE_c correspond to the change in the absolute energy of step (c) of the reaction scheme (6). The angular values correspond to the angle $\angle(\mathrm{X}\cdots\mathrm{H}\cdots\mathrm{O}) = 180° - \xi$. Raw absolute energy data are reported in Table S5 the Supporting Information.

Solvent effects have a relatively weak impact on the global conformation of **RAH** in both reactive and transition state clusters. However, they do significantly alter the distances of the transition state $\mathrm{X}\cdots\mathrm{H}\cdots\mathrm{O}$ bridges, distances that are now resulting in clear asymmetry. Specifically, the bond lengths $\mathrm{X}\cdots\mathrm{O}$ and $\mathrm{X}\cdots\mathrm{H}$ are 1.47/1.09 Å (hydrazine) and 1.23/1.13 Å(DEHA), regardless of T (*i.e.* regardless of the water dielectric constant). Furthermore, solvent effects weaken the energy barriers $\Delta E^{\ddagger}$ by about $\delta E(\epsilon) = 3.4\,\mathrm{kcal\,mol^{-1}}$ for hydrazine and $2.2\,\mathrm{kcal\,mol^{-1}}$ for DEHA. The dependence of the $\delta E(\epsilon)$ value and the cluster harmonic frequencies on the water dielectric constant ϵ are weak. For both **RAH**'s, the $\delta E(\epsilon)$ value decreases by only $0.1\,\mathrm{kcal\,mol^{-1}}$ as ϵ

decreases from 78 to 25 and the harmonic frequencies in bulk water differ at most by $5\,\mathrm{cm}^{-1}$ compared to their counterparts in gas phase, on average. We then estimate the thermal corrections $\Delta G_{\mathrm{thermal}}/\Delta\tilde{G}_{\mathrm{thermal}}$ from gas phase frequency data. Note that the latter corrections are almost insensitive (within 0.2 kcal mol^{-1}) to the frequency scaling factor value used (from 0.85 to 1.0).

From the data summarized in Table 1, the thermal corrections $\Delta G_{\mathrm{thermal}}/\Delta\tilde{G}_{\mathrm{thermal}}$ have a significant effect on the $\Delta G^{\ddagger}$ barriers. $\Delta G_{\mathrm{thermal}}$ are systematically larger by 2 to 3 kcal mol^{-1} compared to $\Delta\tilde{G}_{\mathrm{thermal}}$ data for both **RAH**'s. However those corrections contributes to further favor the reactivity of hydrazine compared to DEHA for all temperatures.

Table 1: Transition state and product cluster absolute energies ΔE and free energies ΔG(T) *wrt* reactive clusters from quantum chemistry computations. ΔE : values in the aqueous phase and in the gas phase (data in italic, for transition state clusters, those energies account for the corrections δE_{CCSD} that amount to +0.3 and +3.1 kcal mol^{-1} for hydrazine and DEHA, respectively). ΔG(T) : values from the thermal corrections $\Delta G_{\mathrm{thermal}}$ and $\Delta\tilde{G}_{\mathrm{thermal}}$ (data in italic). Regarding products, the energy values are pure UM06-2X/aug-cc-pVTZ + D3 data. All energies in kcal mol^{-1}.

Transition state	$[N_2H_4, O_2]^{\ddagger}$	$[(C_2H_5)_2NOH, O_2]^{\ddagger}$
$\Delta E^{\ddagger}$	24.7 *28.2*	20.6 *22.7*
$\Delta G^{\ddagger}$(300K)	23.9 *22.9*	21.4 *19.4*
$\Delta G^{\ddagger}$(350K)	24.5 *23.4*	22.1 *19.8*
$\Delta G^{\ddagger}$(400K)	25.1 *23.5*	22.9 *20.2*
$\Delta G^{\ddagger}$(450K)	25.7 *23.9*	23.7 *20.6*
$\Delta G^{\ddagger}$(500K)	26.3 *24.2*	24.5 *21.0*
$\Delta G^{\ddagger}$(550K)	26.9 *24.5*	25.3 *21.5*
Product	$[N_2H_3^{\bullet}, HO_2^{\bullet}]^{p}$	$[(CH_3CH_2)_2NO^{\bullet}, HO_2^{\bullet}]^{p}$
$\Delta E^{\ddagger}$	19.4 *21.1*	13.2 *15.7*

3.3 Propensity of O_2 for hydrazine and DEHA in the aqueous phase and reactive conformations from MD simulations

We define the propensity of O_2 for hydrazine and DEHA in the aqueous phase from the main features of the hydrazine/O_2 and DEHA/O_2 PMFs in liquid water as computed according to our

simulation protocol. Specifically, the O_2 propensity is related to the characteristics of the first minima in the PMFs. A deeper minimum at short intermolecular distances indicates a stronger propensity. The PMFs for temperatures ranging from 300 to 550 K are plotted as a function of the inter-molecular distances R defined in Section 2.6 in Figure 6. To align the PMF profiles, we shift them so that they are zero at $R_{\text{shift}} = 9.5$ Å. The uncertainty associated with the PMF values is approximately 0.1 kcal mol^{-1}.

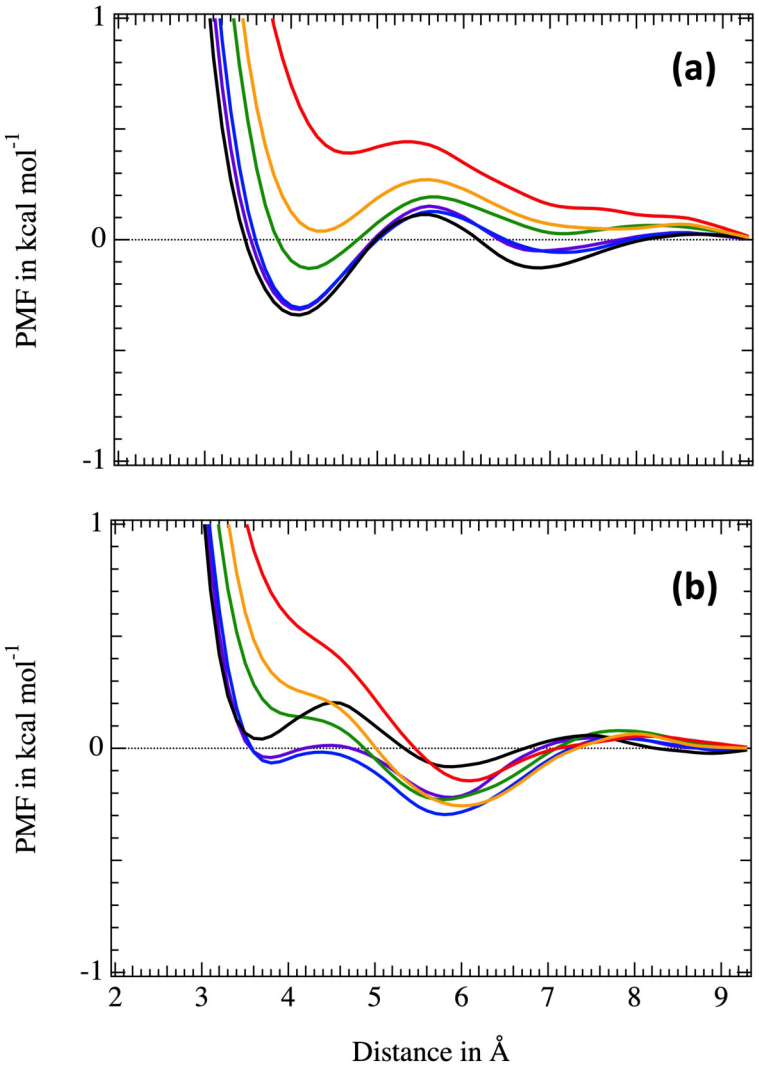

Figure 6: Hydrazine/O_2 (a) and DEHA/O_2 (b) PMFs in the aqueous phase as a function of the inter molecular distance R. PMFs from 300 to 550 K are shown by bold lines from black to red. All PMFs are shifted to be zero at $R_{shift} = 9.5$ Å.

From 300 to 400 K, the PMF profiles for hydrazine are nearly identical within the computational uncertainties. These PMFs exhibit a consistent pattern: a first minimum at approximately 4.1 Å, followed by a maximum at around 5.5 Å, and a second minimum at approximately 6.9 Å. The depths of the latter minima are -0.35 and $-0.10\,\mathrm{kcal\,mol^{-1}}$, respectively, whereas the height of the first maximum is $+0.15\,\mathrm{kcal\,mol^{-1}}$. Notably, these features of the hydrazine PMFs at low temperatures align with those observed for the methane dimer in the aqueous phase.[38] At higher temperatures, the O_2 propensity for hydrazine decreases: the energy depth of the PMF first minimum decreases from 450 K up to be positive at 550 K (by $+0.5\,\mathrm{kcal\,mol^{-1}}$). The propensity of O_2 for hydrazine is thus almost equal until 400 K and then it starts to noticeably decrease. To assess the reliability of the hydrazine/O_2 PMFs, we performed simulations using an alternative set of hydrazine/water force field parameters that yield a weaker solvation free energy (ΔG_{solv}) value for hydrazine, differing by $1\,\mathrm{kcal\,mol^{-1}}$ compared to our original parameter set. Specifically, we modified the parameters of the U^{lh} term, resulting in binding energies of the hydrazine/water dimer of -7.1 and $-6.4\,\mathrm{kcal\,mol^{-1}}$ for the original and altered parameter sets, respectively. The PMFs computed using the alternative parameter set matched the previously described PMFs obtained with the original parameters (see Figure S9 of the Supporting Information).

The DEHA PMFs clearly differ from the hydrazine ones. If they present a weak first minimum located at about 3.7 Å up to 400 K, that minimum vanishes at higher temperatures. Moreover that minimum (when it exists) is less stable than the second one located at about 6 Å, which exists at all temperatures and whose depth is comparable to that of the hydrazine PMF first minimum.

The spatial domain corresponding to the PMF first minima is a sphere of radius $R_1 = 5.5$ Å (hydrazine, up to 550 K) and $R_1 = 4.7$ Å (DEHA, up to 400 K). We assume the probability $p_a(\mathrm{T})$ of O_2 presence in the sphere corresponding to the latter first PMF minima to be the association probability of **RAH** and O_2 in solution at a temperature T. We compute $p_a(\mathrm{T})$ according to

$$p_a(\mathrm{T}) = \frac{1}{Z}\int_0^{R_1} \exp\left[-\beta \mathrm{PMF}(r)\right] r^2 dr, \tag{20}$$

here, β is the Boltzmann factor and Z is a normalization factor that we define as

$$Z = \int_0^{R_{shift}} \left[\exp\left(-\beta \mathrm{PMF}(r)\right) - 1\right] r^2 dr + \bar{\mathrm{V}}. \tag{21}$$

Here, $\bar{\mathrm{V}}$ is the mean volume of the cubic simulation cell at temperature T. Our definition for Z yields the probability to find one O_2 molecule per MD simulation box to be normalized.

The p_a(T) values are summarized in Table 2. Overall, these values are weak and exhibit a decreasing trend with increasing temperature. For hydrazine, the p_a values range from approximately 1.2 to 2 %, while for DEHA, they range from about 0.6 to 0.8 %. Importantly, the simulations reveal that the probability of O_2 being in close proximity to hydrazine is approximately 2.3 times higher than for DEHA, irrespective of temperature. This indicates a stronger propensity of O_2 towards hydrazine compared to DEHA in diluted DEHA/hydrazine-O_2 aqueous solutions, at the scale of 0.05 M.

Table 2: Probabilities p_a and ratios p_r for hydrazine and DEHA. The values p_r are here computed from the parameter set $(\delta r, \xi) = (0.4\,\text{Å}, 45°)$. The uncertainties regarding p_r values amounts to ±15 % (DEHA) and ±2 % (hydrazine). Regarding p_a values, they amount to at most ±5 %, regardless of RAH. $\bar{\mathrm{V}}$ is the mean volume of the simulation cell along our NPT simulations (the volume uncertainty is ± 0.1 nm^3).

T (K)	$\bar{\mathrm{V}}$ (nm^3)	p_a (in %)		p_r (in %)	
		hydrazine	DEHA	hydrazine	DEHA
300	29.9	2.03	0.86	22.1	0.1
350	30.4	1.62	0.73	23.5	0.2
400	31.3	1.58	0.72	24.5	0.5
450	32.7	1.48	0.68	25.2	0.8
500	34.4	1.41	0.63	25.3	0.8
550	36.8	1.30	0.58	24.3	1.4

To further investigate **RAH**/O_2 conformations in liquid water, we performed two new series of NPT MD simulations for T ranging from 300 to 550 K and along which we harmonically restrained the intermolecular distance R to target values R_c corresponding to the location of the PMF first minimum for hydrazine and DEHA as observed at T $\leq$ 400 K. These new simulations were per-

formed at the 50 ns scale and sampled each 5 ps. We post process them according to the clustering protocol detailed in Section 2.7 to identify the main **RAH**/O_2 conformational clusters.

Figure 7 shows representative geometries of the eight most abundant hydrazine/O_2 clusters identified at 300 K, which account for 92 % of all the sampled conformations. At higher temperatures, the number of identified clusters decreases to five at 550 K (see Figures S10 and S11 of the Supporting Information). However, these clusters can be regarded as sets of clusters identified at 300 K. Within the 300 K clusters, the shortest oxygen/nitrogen distance ranges from 3.24 to 3.74 Å. As expected, this distance increases with increasing temperature, reaching a range of approximately 3.40 to 3.95 Å for 550 K clusters. These distances are consistent with those observed in the hydrazine/O_2 reactive cluster in the gas phase (as discussed in Section 3.2). The mean angle value between the NN and O_2 axes in all clusters, regardless of T, varies from 29 to 84°. From visual inspections of the cluster conformations, it can be observed that at least one of the hydrazine hydrogens typically lies in close proximity to one of the oxygen atoms of O_2.

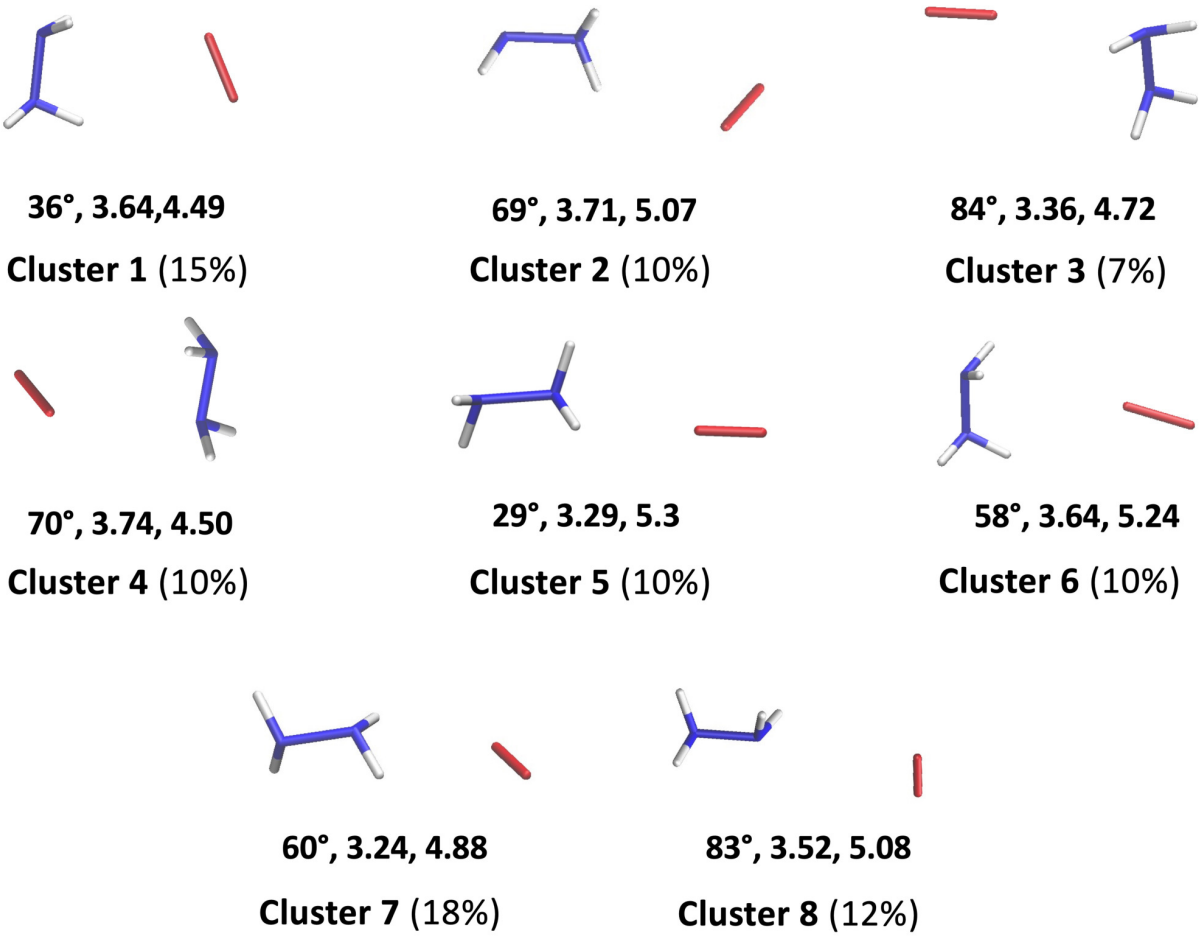

Figure 7: Most abundant hydrazine/O_2 clusters at 300 K corresponding to the hydrazine/O_2 PMF first minimum in the aqueous phase. The structures shown correspond to the center of mass of the cluster distribution. In parentheses, the cluster relative abundance. Data in bold characters correspond to the mean angle between the NN and the O_2 axes and to the shortest and longest O_2/nitrogen distances (in Å).

For DEHA, the number of identified clusters is generally lower compared to hydrazine at all temperatures, ranging from five at 300 K down to three at 550 K. Importantly, the most abundant DEHA/O_2 geometries do not correspond to a reactive conformation where O_2 is in close proximity to the DEHA hydroxyl amine hydrogen. Instead, in the four most abundant clusters at 300 K, O_2 interacts at short range with the hydrophobic ethyl side groups of DEHA rather than with the hydroxyl amine hydrogen. Figure 8 provides visual representations of these DEHA/O_2 clusters.

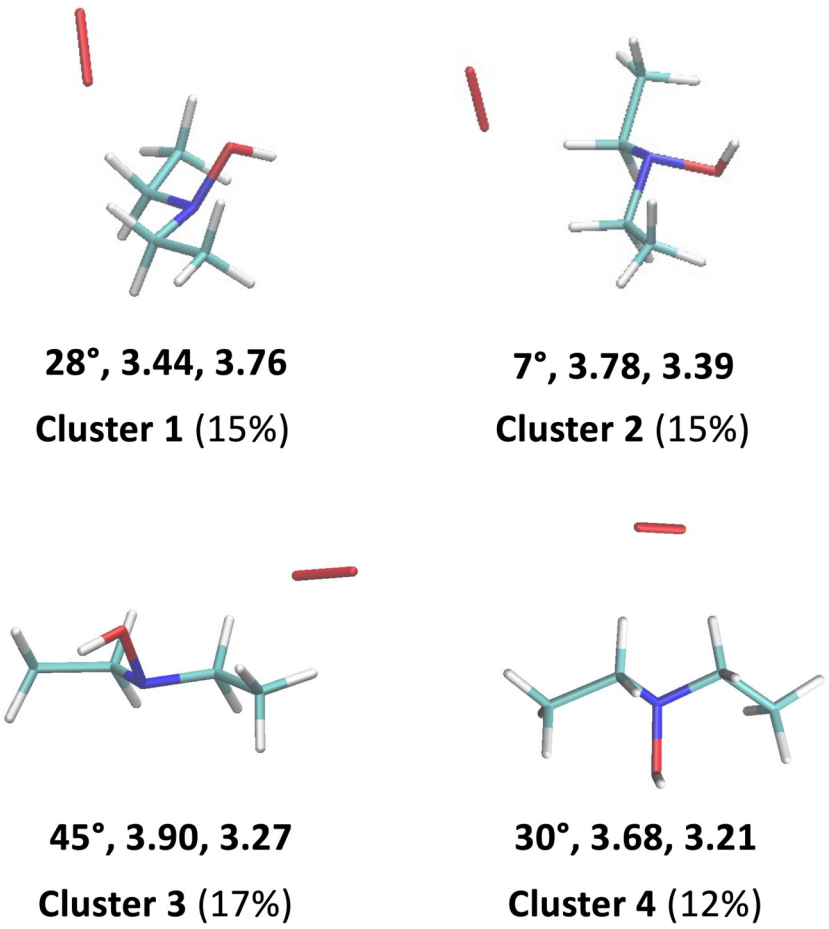

Figure 8: The four most abundant DEHA/O_2 clusters at 300 K corresponding to the PMF first minimum in the aqueous phase. The structures shown correspond to the center of mass of the cluster distribution. In parentheses, the cluster relative abundance. Data in bold characters correspond to the mean angle between the NO and the O_2 axes and to the shortest O_2/oxygen O_2/nitrogen distances (in Å).

We quantify the proportion p_r of [**RAH**,O_2] conformations that are in potential reactive geometry as the proportion of conformations in which a least one single **RAH** hydrogen-O_2 oxygen pair obeys:

1. the atom pair distance is smaller than $r_{\max}$,

2. the angle ξ between the vectors **XH** and **HO** (X and H belonging to hydrazine or to the DEHA hydroxyl amine moiety) is smaller than $\xi_{\max}$.

r_{max} and $\xi_{\max}$ are two arbitrary parameters whose magnitude are inferred from the quantum chemistry geometries of reactive and transition state clusters. From the discussions of Section 3.2, the shortest equilibrium distance $r^{\mathrm{q}}_{\min}$ between a **RAH** reactive hydrogen and an O_2 oxygen is about 2.3 Å (hydrazine) and 2.6 Å (DEHA). In transition state clusters, the angle ξ is 41 (hydrazine) and 22° (DEHA). That yields us to consider here a set of three $\xi_{\max}$ values, namely: 25, 45 and 60°. We also consider a set of three values $r_{\max}$: they correspond to the above $r^{\mathrm{q}}_{\min}$ values to which we add δr =+0.2, +0.4 and +0.6 Å.

The p_r data for $(\delta r, \xi_{\max}) = (0.4\,\text{Å}, 45°)$ are summarized in Table 2 (all the data p_r and the exact **RAH** hydrogen-O_2 oxygen radial distribution functions are reported in Table S6 and Figure S12 of the Supporting Information). The values p_r are about 24.0 ± 1.0 % (hydrazine) and 0.1 ± 0.1 % (DEHA) for the latter parameter set $(\delta r, \xi_{\max})$, regardless of T. They are three times weaker for ξ_{max} =25°, and twice as large for ξ_{max} = 60°, regardless of the compound, T and δr. Lastly, for a given ξ_{max} value, the values p_r increase by a factor of 1.5 as δr increases, regardless of T and the compound.

In Figure 9, we plot the largest and weakest ratios (on average) of p_r values, computed from all the parameters $(\delta r, \xi_{\max})$, between hydrazine and DEHA as a function of T. We also include the mean ratio computed over the full parameter sets and the ratio corresponding to the parameter set $(\delta r, \xi_{\max})$ =(0.4 Å, 45°). It can be observed that all of these ratios follow exponential decay functions of T, and they decrease as the value of $\xi_{\max}$ increases. Importantly, the ratios indicate that hydrazine clusters in a reactive conformation are more abundant at any temperature compared to DEHA clusters, regardless of the choice of the parameter set $(\delta r, \xi_{\max})$. Additionally, the mean ratio of p_r values is close to that computed from the parameter set (0.4 Å, 45°), which suggests that

this parameter set is a reasonable choice for investigating reactive conformations for both hydrazine and DEHA.

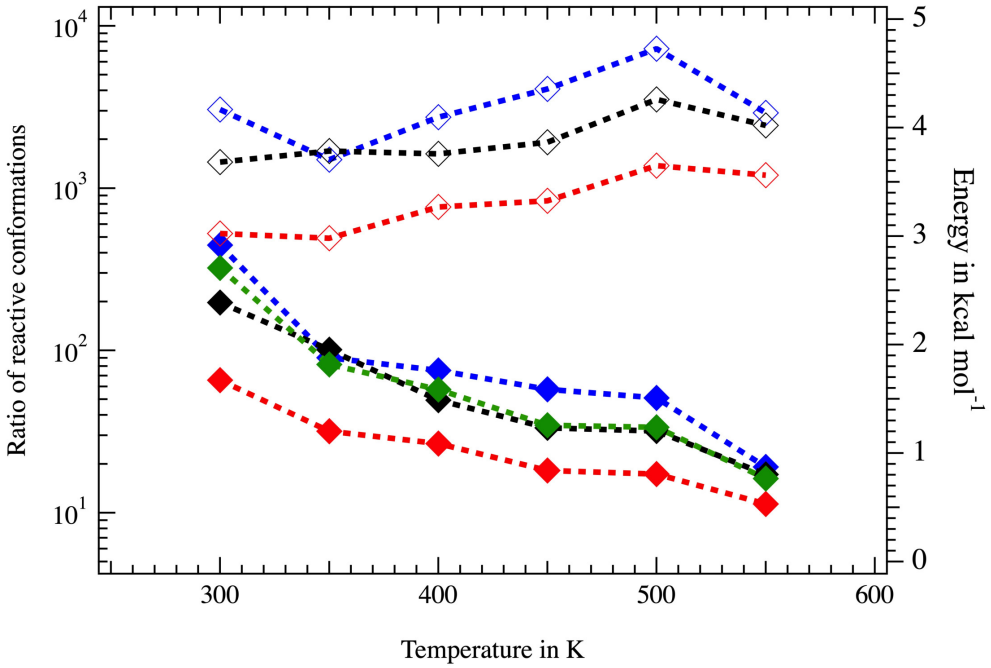

Figure 9: Left axis and full symbols : ratios of the proportion p_r (between hydrazine and DEHA) as a function of T for the parameter sets $(\delta r, \xi_{\max}) = (0.6\,\text{Å},\ 60°)$, $(0.2\,\text{Å},\ 25°)$, $(0.4\,\text{Å},\ 45°)$ in red, blue and black symbols, respectively. Right axis and open symbols : DEHA-hydrazine differences in free energy values $G_{\text{conformation}}$ computed from the latter three p_r ratios. In green symbols (left axis) the mean ratio of p_r values computed from all the parameter sets $(\delta r, \xi_{\max})$.

The weaker proportion of [DEHA,O_2] reactive clusters as compared to hydrazine, can be attributed to the hydrophobic nature of O_2, a species that prefers to interacts at short range from **RAH** hydrophobic moieties to minimize the destabilizing effects induced by its presence on the solvent water and on the local interaction network between water and the DEHA hydroxyl amine moiety.

3.4 First proton abstraction rate constants

We define the free energy quantity $G_{\text{conformational}} = -\text{RT} \ln \left[p_r p_a/(1-p_a)^2\right]$ from which we rewrite the rate constants $k(\text{T})$ of Equation (7) as

$$k(\mathrm{T}) = \frac{\mathrm{k_B T}}{hc_0} \exp\left[-\beta\left(\Delta G^{\ddagger} + G_{\mathrm{conformational}}\right)\right]. \tag{22}$$

The rate constants for hydrazine and DEHA are plotted as a function of T in Figure 10 from $G_{\mathrm{conformational}}$ data computed using the geometrical index set $(\delta r, \xi_{max}) = (0.4\,\text{Å}, 45°)$.

The electronic density reorganization effects tied to the proton transfer from **RAH** to O_2 are measured by the quantity $\Delta G^{\ddagger}$, whereas the quantity $G_{\mathrm{conformational}}$ is a thermodynamic measure of the weight of conformational effects (usually referred as steric effects) on the first proton abstraction reactions here investigated. The ratio of the rate constants $k(\mathrm{T})$ between hydrazine and DEHA depends on the differences $\Delta\Delta G^{\ddagger}$ and $\Delta G_{\mathrm{conformational}}$ in the $\Delta G^{\ddagger}$ and $G_{\mathrm{conformational}}$ values between both compounds.

We plot in Figure 9 the differences $\Delta G_{\mathrm{conformational}}$ as a function of T for the three sets of geometric indexes $(\delta r, \xi_{max})$ discussed in the above Section 3.3. The values $\Delta G_{\mathrm{conformational}}$ slightly depend on T and on the latter indexes : they vary from about -2.9 (300 K) up to $-4.1\,\mathrm{kcal\,mol^{-1}}$ (550 K). On average and regardless of T, $\Delta G_{\mathrm{conformational}}$ is about $-4.0 \pm 0.3\,\mathrm{kcal\,mol^{-1}}$, a value that cancels out the differences $\Delta\Delta G^{\ddagger}$ between hydrazine and DEHA at any temperature. Accounting for the two sets of thermal corrections $\Delta G_{\mathrm{thermal}}$ and $\Delta \tilde{G}_{\mathrm{thermal}}$, that consequently yields the first proton abstraction rate constants for hydrazine and DEHA to be similar ($\Delta \tilde{G}_{\mathrm{thermal}}$) or larger for hydrazine ($\Delta G_{\mathrm{thermal}}$), as depicted in Figure 10, irrespective of temperature. In other words, the reactivity of DEHA towards O_2 is unfavorably affected by conformational (steric) effects, leading to an approximately 30-fold increase in the magnitude of its constant $k(\mathrm{T})$ compared to hydrazine. On the other hand, the proton transfer from hydrazine to O_2 is more hindered compared to DEHA.

We determine the activation energies $\tilde{E}_a$ for the first proton abstraction reactions by fitting the rate constants $k(\mathrm{T})$ to the Arrhenius equation. Regardless of the thermal corrections, the estimated best values for both **RAH**'s are $\tilde{E}_a = 21.5 \pm 1.5\,\mathrm{kcal\,mol^{-1}}$. The uncertainty takes into account all the discussed uncertainties as well as the interpolation uncertainty associated with the raw $k(\mathrm{T})$ data. Interestingly, the lower bound of our estimated $\tilde{E}_a$ value for DEHA overall aligns with the higher estimate bound of the experimental apparent activation energy for the complete O_2

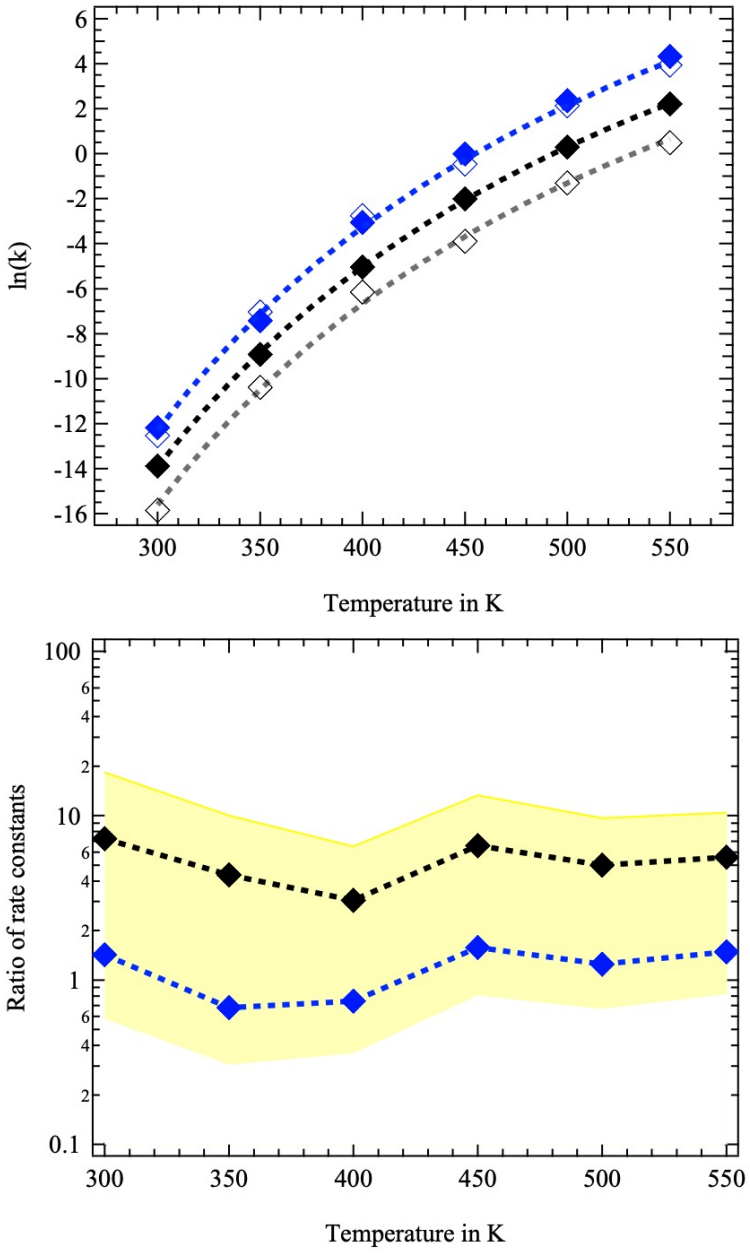

Figure 10: Top: Neperian logarithm of the rate constants of the first proton abstraction process for hydrazine (full symbols) and DEHA (empty symbols) as a function of T. Rate constants in black and blue symbols are computed from the quantities $\Delta G_{\text{thermal}}$ and $\Delta \tilde{G}_{\text{thermal}}$, respectively. In dashed lines the best Arrhenius functions extrapolated from the rate constant data (for readability purpose, the Arrhenius plot for hydrazine based on $\Delta \tilde{G}_{\text{thermal}}$ data is not shown). Down: ratio of the rate constants between hydrazine and DEHA from $\Delta G_{\text{thermal}}$ (black symbols) and $\Delta \tilde{G}_{\text{thermal}}$ (blue symbols). The yellow domain delimits the range of possible ratios as taking into account all the sources of uncertainty.

scavenger process in solution, as reported by Buxton and Stuart,[9] which is $16.7 \pm 1.2\,\mathrm{kcal\,mol^{-1}}$, and it is larger but within the same order of magnitude as the experimental estimate reported by Shaffer and Heicklen[11], despite their experimental value corresponding to a potentially different O_2 scavenger process mechanism depicted in Eqn. 2.

Regarding the ratio of the rate constants $k(\mathrm{T})$ for the first proton abstraction reactions between hydrazine and DEHA, it spans between 4 and 7 from $\Delta G_{\mathrm{thermal}}$ data, whereas it amounts to about 1 as accounting for $\Delta \tilde{G}_{\mathrm{thermal}}$ values, regardless of T. Our latter two ratios nicely bound the experimental estimate (approximately 3) of the rate constant ratio between hydrazine and DEHA for the complete O_2 scavenger process in solution, as recently reported by Jäppinen et al.[5].

In summary, our data support a O_2 scavenger process that relies on an initial rate-determining step corresponding to the first proton abstraction reaction from **RAH** to O_2, resulting in the formation of radicals $\mathbf{RA}^{\bullet}$ and $HO_2^{\bullet}$. Therefore, our simulations endorse the interpretation of kinetic data for the O_2 scavenger process involving **RAH** compounds such as hydrazine and DEHA using the simple kinetic equation $k(\mathrm{T})[\mathbf{RAH}][O_2]$, as in the recent experimental study by Jäppinen et al.[5].

4 Conclusion

We detailed a comprehensive theoretical protocol combining quantum chemistry methods and MD simulations to investigate the initial stages of the O_2 scavenger process in the aqueous phase of hydrazine and DEHA, *i.e.* the proton first abstraction reactions from a reducing agent **RAH** that yields the radical $HO_2^{\bullet}$. Quantum chemistry methods are utilized to study the proton transfer from an associated [**RAH**,O_2] cluster in a reactive conformation. Furthermore, these methods provide valuable data for determining the parameters of the force field used in the subsequent MD simulations. Using MD simulations, we estimate the probability of the **RAH** and O_2 species to be associated in a reactive geometry. It is assumed that the first proton abstraction processes occur at a sufficiently slow rate, allowing the **RAH**/O_2 association to reach equilibrium before the reaction takes place. In our present study, we have applied this theoretical protocol to compare the behavior of hydrazine and DEHA as O_2 scavengers over a temperature range spanning from 300 K up to

550 K.

Our findings reveal that the first proton abstraction reaction of hydrazine is influenced by conformational effects. In other words, the probability of observing a reactive cluster [hydrazine, O_2] in solution is higher than for DEHA, due to these conformational effects. On the other hand, the electronic density reorganization effects associated with the proton transfer from **RAH** to O_2 favor DEHA. Interestingly, the magnitudes of these opposing effects counterbalance each other, resulting in similar rate constants $k(\mathrm{T})$ for the first proton abstraction reactions of hydrazine and DEHA. This holds true regardless of the temperature under consideration.

The two O_2 scavenger mechanisms considered to interpret experimental data are based on a complex chain of reactions, as depicted in Equations (2) and (5). In a chain mechanism, the experimental apparent activation energy E_a is generally a weighted average of the standard state enthalpies of all the intermediate, transition state, and product entities involved in the reaction mechanism.[53,54] Assuming that the first proton abstraction reaction is the rate-determining step of the hydrazine and DEHA O_2 scavenger process in solution, the overall agreement between our activation energies $\tilde{E}_a$ and the experimental estimates suggests that the subsequent chain steps are rapid and lead to intermediate stable compounds that possess similar stability as the initial reactants. That hypothesis is supported by the quantum chemistry data presented by Asgharzade et al.[10], which show that the most stable forms of the reactants and of the intermediate states of the hydrazine/O_2 reaction in the gas phase (resulting in the HNNH and $H_2N_2(OH)_2$ compounds) exhibit nearly isoenergetic behavior within a few kcal mol^{-1}.

Based on our extensive quantum chemistry calculations and MD simulations, we provide support for the interpretation of experimental data concerning the O_2 scavenger process involving **RAH** species such as hydrazine and DEHA in the aqueous phase. The simple kinetic equation $k(\mathrm{T})[\mathbf{RAH}][O_2]$ appears to be a suitable approach for describing the observed kinetics. Furthermore, our MD simulations demonstrate that **RAH** compounds containing non-reactive hydrophobic groups (such as the ethyl groups in DEHA) may not be inherently well-suited as efficient O_2 scavengers in bulk water. This is because in the aqueous environment, O_2 tends to interact more favorably with hydrophobic groups rather than potential reactive **RAH** moieties, such as the hydroxylamine group in DEHA. However, this conformational (steric) artifact can be compensated for

by considering compounds that contain reactive functional groups favoring direct proton transfer reactions with O_2.

Lastly we make use here of a sophisticated polarizable force field to investigate the association properties of O_2 with hydrazine and DEHA in liquid water. That may be also achieved using standard non polarizable force fields (once a reliable set of parameters is available). Moreover and to our opinion, comparing our own data to results based on standard force fields is an interesting route to estimate the uncertainty regarding molecular association tied to the force field sophistication. We made in the present study a comparison between the hydration structural properties of hydrazine predicted by our polarizable approach and earlier findings from standard force fields. Even if we point out differences, in all both kinds of force fields provide a close description of hydrazine hydration, which suggests that investigating early steps of chemical reactions may be also achieved using standard molecular modeling approaches.

Supporting Information Available

Details about the quantum CBS scheme, unpublished experimental data regarding hydrazine and DEHA thermal decomposition, the Cartesian coordinates and quantum energy raw data of the reactive and transition antioxidant/O_2 clusters, force field parameters, as well as several simulation results discussed in the main manuscript are provided as the Supporting Information.

Acknowledgments

The authors thank EDF and CEA for the financial support of this study in the framework of contract I3P-2020 F35158. VV acknowledges support from PIA ANR project CaPPA (ANR-11-LABX-0005-01), I-SITE ULNE projects OVERSEE and MESONM International Associated Laboratory (LAI) (ANR-16-IDEX-0004), and the French Ministry of Higher Education and Research, region Hauts de France council and European Regional Development Fund (ERDF) projects CPER CLIMIBIO and WaveTech.

References

(1) Frayne, C. *Boiler Water Treatment: Principles and Practice*; Chemical Publishing Company, 2002.

(2) *Proposal for Identification of a Substance As a Category 1a or 1b CMR, PBT, vPvB or a Substance of an Equivalent Level of Concern*; 2011; Annex XIV of REACH, European Chemical Agency on request of the European Commission.

(3) Rahman, M. M.; Al-Sulami, S. A.; Almauili, F. A. Carbohydrazide vs Hydrazine: A Comparative Study. *PowerPlant Chemistry* **2018**, *20(1)*.

(4) Al Helal, A.; Soames, A.; Gubner, R.; Iglauer, S.; Barifcani, A. Performance of Erythorbic Acid as an Oxygen Scavenger in Thermally Aged Lean MEG. *J. Petrol. Sci. Eng.* **2018**, *170*, 911–921, DOI: 10.1016/j.petrol.2018.06.073.

(5) Jäppinen, E.; Ikäläinen, T.; Lindfors, F.; Saario, T.; Sipilä, K.; Betova, I.; Bojinov, M. A comparative study of hydrazine alternatives in simulated steam generator conditions—Oxygen reaction kinetics and interaction with carbon steel. *Electrochim. Acta* **2021**, *369*, 137697, DOI: 10.1016/j.electacta.2020.137697.

(6) Cáceres, T.; Lissi, E. A.; Sanhueza, E. Autooxidation of Diethyl Hydroxylamine. *Int. J. Chem. Kinet.* **1978**, *10*, 1167–1182, DOI: 10.1002/kin.550101107.

(7) Fruzzetti, K.; Marks, C. *International Conference on Water Chemistry of Nuclear Reactors (NPC - 2018), San Francisco United States*; 2018.

(8) *Hydrazine Alternatives for the Pressurized Water Reactor/Pressurized Heavy Water Reactor Secondary System: Diethylhydroxylamine (DEHA) Decomposition and Deaeration Kinetics*; 2022; EPRI, Palo Alto, CA, 3002023967.

(9) V. Buxton, G. V.; Stuart, C. R. Radiation Chemistry of Aqueous Solutions of Hydrazine at Elevated Temperatures Part 2.—Solutions Containing Oxygen. *J. Chem. Soc., Faraday Trans.* **1997**, *93*, 1535–1538, DOI: 10.1039/A608040E.

(10) Asgharzade, S.; Vahedpour, M.; Douroudgari, H. Theoretical Study on the Mechanism of the N_2H_4 plus O_2 Reaction on the Singlet and Triplet Potential Energy Surfaces. *Comput. Theor. Chem.* **2017**, *1104*, 47–55, DOI: 10.1016/j.comptc.2017.02.007.

(11) Shaffer, D.; Heicklen, J. Oxidation of Diethylhydroxylamine in Water Solution at 25-80 Degree. *J. Phys. Chem.* **1986**, *90*, 4408–4413, DOI: 10.1021/j100409a039.

(12) Ishida, K.; Wada, Y.; Tachibana, M.; Aizawa, M.; Fuse, M.; Kadoi, E. Hydrazine and Hydrogen Co-injection to Mitigate Stress Corrosion Cracking of Structural Materials in Boiling Water Reactors, (I) Temperature Dependence of Hydrazine Reactions. *J. Nucl. Sci. Technol.* **2006**, *43*, 65–76, DOI: 10.1080/18811248.2006.9711068.

(13) Plugatyr, A.; Svishchev, I. M. Stability of Hydrazine, Morpholine and Ethanolamine at 275° C and In Situ Measurement of Redox and Acid–Base Properties. *Proceedings of Nuclear Plant Chemistry Conference 2010 (NPC 2010) October 3-7, in Quebec* **2010**,

(14) Million-Picallion, L.; Berger, G.; Lefèvre, G.; Delaunay, S.; Mansour, C. Stability of Hydrazine, Morpholine and Ethanolamine at 275° C and In Situ Measurement of Redox and Acid–Base Properties. *Journal of Solution Chemistry* **2015**, *44*, 1900–1919, DOI: 10.1007/s10953-015-0375-4.

(15) Tomasi, J.; Mennucci, B.; Cammi, R. Quantum Mechanical Continuum Solvation Models. *Chem. Rev.* **2005**, *105*, 2999–3094, DOI: 10.1021/cr9904009.

(16) Frisch, M. J.; Trucks, G. W.; Schlegel, H. B.; Scuseria, G. E.; Robb, M. A.; Cheeseman, J. R.; Scalmani, G.; Barone, V.; Petersson, G. A.; Nakatsuji, H. et al. Gaussian˜16 Revision C.01. 2016; Gaussian Inc. Wallingford CT.

(17) Zhao, Y.; Truhlar, D. G. The M06 suite of density functionals for main group thermochemistry, thermochemical kinetics, noncovalent interactions, excited states, and transition elements: two new functionals and systematic testing of four M06-class functionals and 12 other functionals. *Theor. Chem. Acc.* **2008**, *120*, 215–241, DOI: 10.1007/s00214-007-0310-x.

(18) Grimme, S.; Ehrlich, S.; Goerigk, L. Effect of the Damping Function in Dispersion Corrected Density Functional Theory. *J. Comput. Chem.* **2011**, *32*, 1456–1465, DOI: 10.1002/jcc.21759.

(19) Kendall, R. A.; Dunning, T. H., Jr.; Harrison, R. J. Electron affinities of the first-row atoms revisited. Systematic basis sets and wave functions. *J. Chem. Phys.* **1992**, *96*, 6796–6806, DOI: 10.1063/1.462569.

(20) Woon, D. E.; Dunning, T. H., Jr. Gaussian basis sets for use in correlated molecular calculations. III. The atoms aluminum through argon. *J. Chem. Phys.* **1993**, *98*, 1358, DOI: 10.1063/1.464303.

(21) Schlegel, H. B. Potential Energy Curves using Unrestricted Møller–Plesset Perturbation Theory with Spin Annihilation. *J. Chem. Phys.* **1986**, *84*, 4530–4534, DOI: 10.1063/1.450026.

(22) Bakowies, D.; von Lilienfeld, O. A. Density Functional Geometries and Zero-Point Energies in Ab Initio Thermochemical Treatments of Compounds with First-Row Atoms (H, C, N, O, F). *J. Chem. Theory Comput.* **2021**, *17*, 4872–4890, DOI: 10.1021/acs.jctc.1c00474.

(23) Temelso, B.; Shields, G. C. The Role of Anharmonicity in Hydrogen-Bonded Systems: The Case of Water Clusters. *J. Chem. Theory Comput.* **2011**, *7*, 2804–2817, DOI: 10.1021/ct2003308.

(24) Zhao, Y.; Truhlar, D. G. Computational Characterization and Modeling of Buckyball Tweezers: Density Functional Study of Concave–Convex$\pi\cdots\pi$ Interactions. *Phys. Chem. Chem. Phys.* **2008**, *10*, 2813–2818, DOI: 10.1039/B717744E.

(25) Brooks, B.; Brooks III, C.; Mackerell, A.; Nilsson, L.; Petrella, R.; Roux, B.; Won, Y.; Archontis, G.; Bartels, C.; Boresch, S. et al. CHARMM: The Biomolecular Simulation Program. *J. Comput. Chem.* **2009**, *30*, 1545–1615, DOI: 10.1002/jcc.21287.

(26) Thole, B. T. Molecular Polarizabilities Calculated with a Modified Dipole Interaction. *Chem. Phys.* **1981**, *59*, 341–350, DOI: 10.1016/0301-0104(81)85176-2.

(27) Réal, F.; Vallet, V.; Flament, J.-P.; Masella, M. Revisiting a Many-Body Model for Water Based on a Single Polarizable Site. From Gas Phase Clusters to Liquid and Air/Liquid Water Systems. *J. Chem. Phys.* **2013**, *139*, 114502, DOI: 10.1063/1.4821166.

(28) Gutowski, K. E.; Gurkan, B.; Maginn, E. J. Force Field for the Atomistic Simulation of the Properties of Hydrazine, Organic Hydrazine Derivatives, and Energetic Hydrazinium Ionic Liquids. *Pure Appl. Chem.* **2009**, *81*, 1799–1828, DOI: doi:10.1351/PAC-CON-08-09-24.

(29) Spelsberg, D.; Meyer, W. Static Dipole Polarizabilities of N_2, O_2, F_2, and H_2O. *J. Chem. Phys.* **1994**, *101*, 1282–1288, DOI: 10.1063/1.467820.

(30) Martyna, G. J.; Tuckerman, M. E.; Tobias, D. J.; Klein, M. L. Explicit Reversible Integrators for Extended Systems Dynamics. *Mol. Phys.* **1996**, *87*, 1117–1157, DOI: 10.1080/00268979600100761.

(31) Toukmaji, A.; Sagui, C.; Borad, J.; Darden, T. Efficient Particle-Mesh Ewald Based Approach to Fixed and Induced Dipolar Interactions. *J. Chem. Phys.* **2000**, *113*, 10913–10927, DOI: 10.1063/1.1324708.

(32) Masella, M. The Multiple Time Step r-RESPA Procedure and Polarizable Potentials Based on Induced Dipole Moments. *Mol. Phys.* **2006**, *104*, 415–428, DOI: 10.1080/00268970500404414.

(33) POLARIS(MD). http://biodev.cea.fr/polaris/, accessed 2023.10.03.

(34) Frenkel, D.; Smit, B. *Understanding Molecular Simulation: From Algorithms to Applications*; Academic Press, 2002; DOI: 10.1063/1.881812.

(35) Warren, G. L.; Patel, S. Hydration Free Energies of Monovalent Ions in Transferable Intermolecular Potential Four Point Fluctuating Charge Water: An Assessment of Simulation Methodology and Force Field Performance and Transferability. *J. Chem. Phys.* **2007**, *127*, 064509, DOI: 10.1063/1.2771550.

(36) Kästner, J.; Thiel, W. Bridging the Gap between Thermodynamic Integration and Umbrella Sampling Provides a Novel Analysis Method: Umbrella Integration. *J. Chem. Phys.* **2005**, *123*, 144104, DOI: 10.1063/1.2052648.

(37) Gonzalez, T. F. Clustering to Minimize the Maximum Intercluster Distance. *Theor. Comput. Sci.* **1985**, *38*, 293–306, DOI: 10.1016/0304-3975(85)90224-5.

(38) Li, J.-L.; Car, R.; Tang, C.; Wingreen, N. S. Hydrophobic Interaction and Hydrogen-Bond Network for a Methane Pair in Liquid Water. *Proc. Natl. Acad. Sci. USA* **2007**, *104*, 2626–2630, DOI: 10.1073/pnas.0610945104.

(39) Asthagiri, D.; Merchant, S.; Pratt, L. R. Role of Attractive Methane-Water Interactions in the Potential of Mean Force between Methane Molecules in Water. *J. Chem. Phys.* **2008**, *128*, 244512, DOI: 10.1063/1.2944252.

(40) Kallikragas, D. T.; Choudhry, K. I.; Plugatyr, A. Y.; Svishchev, I. M. Diffusivity and Hydration of Hydrazine in Liquid and Supercritical Water through Molecular Dynamics Simulations and Split-Flow Pulse Injection Experiments. *J. Chem. Phys.* **2013**, *139*, 134507, DOI: 10.1063/1.4823513.

(41) Thapa, S. K.; Adhikari, N. P. A Molecular Dynamics Study of Oxygen Gas in Water at Different Temperatures. *Int. J. Mod. Phys. B* **2013**, *27*, 1350023, DOI: 10.1142/S0217979213500239.

(42) Vizoso, S.; Heinzle, M. G.; Rode, B. M. Hydroxylamine–Water: Intermolecular Potential Function and Simulation of Hydrated NH2OH. *J. Chem. Soc., Faraday Trans.* **1994**, *90*, 2337–2344, DOI: 10.1039/FT9949002337.

(43) Ferreira de Lima, G.; Pliego, J. R.; Anderson Duarte, H. Stability of Hydroxylamine Isomers in Aqueous Solution: Ab Initio Study using Continuum, Cluster-Continuum and Shells Theory of Solvation. *Chem. Phys. Lett.* **2011**, *518*, 61–64, DOI: 10.1016/j.cplett.2011.11.001.

(44) Salvitti, G.; Baroncelli, F.; Nicotri, C.; Evangelisti, L.; Melandri, S.; Maris, A. How Water Interacts with the NOH Group: The Rotational Spectrum of the 1:1 N,N-diethylhydroxylamine · Water Complex. *Molecules* **2022**, *27*, 8190, DOI: 10.3390/molecules27238190.

(45) Marenich, A. V.; Kelly, C. P.; Thompson, J. D.; Hawkins, G. D.; Chambers, C. C.; Giesen, D. J.; Winget, P.; Cramer, C. J.; Truhlar, D. G. *Minnesota Solvation Database - version 2012*; University of Minnesota, Minneapolis, 2012.

(46) Vácha, R.; Slavíček, P.; Mucha, M.; Finlayson-Pitts, B. J.; Jungwirth, P. Adsorption of Atmospherically Relevant Gases at the Air/Water Interface: Free Energy Profiles of Aqueous Solvation of N_2, O_2, O_3, OH, H_2O, HO_2, and H_2O_2. *J. Phys. Chem. A* **2004**, *108*, 11573–11579, DOI: 10.1021/jp046268k.

(47) Garrett, B. C.; Schenter, G. K.; Morita, A. Molecular Simulations of the Transport of Molecules across the Liquid/Vapor Interface of Water. *Chem. Rev.* **2006**, *106*, 1355–1374, DOI: 10.1021/cr040370w.

(48) Wilhelm, E.; Battino, R.; Wilcock, R. J. Low-Pressure Solubility of Gases in Liquid Water. *Chem. Rev.* **1977**, *77*, 219–262, DOI: 10.1021/cr60306a003.

(49) Wildman, S. A.; Crippen, G. M. Prediction of Physicochemical Parameters by Atomic Contributions. *J. Chem. Inf. Comput. Sci.* **1999**, *39*, 868–873, DOI: 10.1021/ci9903071.

(50) *NIST Chemistry Web Book : The NIST reference data base n. 69*; P.J. Linstrom et W.G. Mallard.

(51) Constantinou, L.; Gani, R. New Group Contribution Method for Estimating Properties of Pure Compounds. *AIChE J.* **1994**, *40*, 1697–1710, DOI: 10.1002/aic.690401011.

(52) Yash, N.; Jurgen, R.; Deresh, R. Estimation of Pure Component Properties: Part 2. Estimation of Critical Property Data by Group Contribution. *Fluid Phase Equilib.* **2007**, *252*, 1–27, DOI: 10.1016/j.fluid.2006.11.014.

(53) Campbell, C. T. The Degree of Rate Control: A Powerful Tool for Catalysis Research. *ACS Catalysis* **2017**, *7*, 2770–2779, DOI: 10.1021/acscatal.7b00115.

(54) Mao, Z.; Campbell, C. T. Apparent Activation Energies in Complex Reaction Mechanisms: A Simple Relationship via Degrees of Rate Control. *ACS Catal.* **2019**, *9*, 9465–9473, DOI: 10.1021/acscatal.9b02761.

TOC Graphic